Calculation of Vertical Stability in an Inverse Aspect-Ratio Expanded Tokamak Plasma Equilibrium

Richard Fitzpatrick [a]

Institute for Fusion Studies, Department of Physics,

University of Texas at Austin, Austin, TX 78712

The stability of vertical modes in an up-down symmetric, aspect-ratio expanded, tokamak plasma equilibrium surrounded by a conformal resistive wall is calculated. The calculation turns out to be significantly different to previous calculations of the stability of non-axisymmetric ideal modes in an aspect-ratio expanded equilibrium. In particular, the role of the toroidal angular momentum flux (which is identically zero for an axisymmetric mode) is instead played by the electromagnetic energy flux. The conservation of electromagnetic energy is used to prove that the perturbed plasma potential energy matrix is Hermitian. Positive triangularity is found to have a strong stabilizing effect on the vertical mode in vertically elongated plasmas, whereas negative triangularity is either destabilizing or weakly stabilizing. It is concluded that finite wall thickness should be taken into account when calculating the maximum controllable plasma elongation of a tokamak plasma.

---

[a] rfitzp@utexas.edu

I. INTRODUCTION

It is well known that an increase in the net toroidal plasma current flowing around a tokamak leads to an enhancement of both the maximum stable β value and the energy confinement time.[1,2] The conventional method of maximizing the total plasma current, without degrading the stability of the system to non-axisymmetric magnetohydrodynamical (MHD) modes, is to modify the plasma's poloidal cross-section such that it is both vertically elongated and triangular.[3] Unfortunately, tokamak plasmas possessing strong cross-sectional shaping are subject to severe axisymmetric instabilities.[4,5] Such instabilities involve bulk vertical motion of the plasma on an Alfvénic timescale (i.e., 10^{-7} s), which results in the sudden and violent termination of the discharge when it comes into contact with the first wall. It is possible to stabilize an axisymmetric mode by placing a perfectly conducting wall around the plasma. In reality, the mode remains unstable because the wall inevitably possesses finite electrical conductivity.[6] However, growth time of the mode is increased from the Alfvén time to the very much longer characteristic L/R time of the wall.[7-9] (See Sect. A 1 for a definition of this time.) Usually, the vacuum vessel plays the role of the wall, and has an L/R time that is well in excess of 10^{-3} s. Such a time is much shorter than the duration of the plasma discharge, but is still long enough to allow active feedback stabilization of the axisymmetric mode with practical power supplies.[10]

Ref. 11 describes the TJ toroidal tearing mode code, which calculates the stability of an inverse aspect-ratio expanded tokamak plasma equilibrium to *non-axisymmetric* tearing modes via asymptotic matching techniques. Ref. 12 describes a generalization of the TJ code that permits it to calculate the stability of the plasma to non-axisymmetric ideal modes in the presence of a perfectly conducting wall surrounding the plasma. (This is possible because the basis solutions used to construct tearing eigenfunctions in TJ can be repurposed to construct ideal eigenfunctions.) The aim of this paper is to describe a further generalization the TJ code that allows it to calculate the stability of the plasma to *axisymmetric* ideal modes in the presence of a resistive wall that surrounds the plasma. It might be hope that, in order to investigate axisymmetric modes, we could simply take the existing TJ code and set the toroidal mode number, n, to zero. Unfortunately, this simple scheme does not work, as

2

evidenced by the large number of terms involving n^{-1} in the analysis of Ref. 11. Hence, as described in Sect. A 3, it is necessary to redo much of the TJ analysis for the special case $n = 0$.

The simplified approach to calculating the vertical stability of tokamak plasmas described in this paper is somewhat different to the simplified approach described in Refs. 13 and 14. In fact, Refs. 13 and 14 employ up-down symmetric, analytic Solov'ev plasma equilibria in which the equilibrium current jumps discontinuously to zero across the plasma-vacuum interface. Such equilibria can have arbitrary aspect-ratios, and possess the simplifying property that the perturbed plasma currents generated by vertical instabilities are surface currents that are localized on the interface. However, Solov'ev equilibria are characterized by very broad current profiles, and, consequently, possess anomalously low normalized plasma inductances, l_i (see Sect. VII E), that can only be varied over a very narrow range. This is problematic because vertical stability is known to have a strong dependence on l_i. (For example, the well-known empirical vertical stability margin for ITER derived in Ref. 15 exhibits an exponential dependence on l_i.) On the other hand, the calculation described in this paper employs realistic diffuse plasma equilibria in which the equilibrium plasma current and pressure go smoothly to zero as the plasma-vacuum interface is crossed, and in which the perturbed plasma currents associated with vertical instabilities are distributed throughout the plasma volume. There is no restriction on the broadness of the current profile, so l_i can be varied over the whole range of values observed in experiments. Our main simplifying approximation is to restrict the inverse aspect-ratio of the plasma to only take small values.

This paper is organized as follows. In Sect. II, we introduce a general axisymmetric plasma equilibrium. In Sect. III, we examine axisymmetric perturbations to this equilibrium. Magnetic perturbations in the vacuum region surrounding the plasma are discussed in Sect. IV. The stability of the equilibrium to ideal axisymmetric modes is examined in Sect. V. The stability of the equilibrium to axisymmetric resistive wall modes is discussed in Sect. VI. The large aspect-ratio approximation is introduced in Sect. VII. The results of the calculations performed with the enhanced version of the TJ code are presented in Sect. VIII. Finally, the paper is summarized in Sect. IX.

II. GENERAL TOKAMAK PLASMA EQUILIBRIUM

All lengths in this paper are normalized to the major radius of the plasma magnetic axis, R_0. All magnetic field-strengths are normalized to the toroidal field-strength at the magnetic axis, B_0. All current densities are normalized to $B_0/(\mu_0\,R_0)$. All plasma pressures are normalized to B_0^2/μ_0. All energies are normalized to $B_0^2\,R_0^3/\mu_0$.

Let R, ϕ, Z be right-handed cylindrical coordinates whose Jacobian is $(\nabla R \times \nabla \phi \cdot \nabla Z)^{-1} = R$. Note that $|\nabla \phi| = 1/R$. The cylindrical axis is assumed to coincide with the symmetry axis of the toroidal plasma equilibrium, which is assumed to have perfectly-nested toroidal magnetic flux-surfaces.

We can write the divergence-free equilibrium magnetic field in the usual Clebsch form [16]

$$\mathbf{B} = \nabla(\phi - q\,\theta) \times \nabla\psi, \tag{1}$$

where ψ is the poloidal magnetic flux enclosed by a given magnetic flux-surface (divided by 2π), $q(\psi)$ the safety-factor profile, and θ a poloidal angle. Note that $\mathbf{B} \cdot \nabla\psi = 0$, which implies that ψ is a flux-surface label. Furthermore, $\mathbf{B} \cdot \nabla(\phi - q\,\theta) = 0$, which implies that the equation of any magnetic field-line in a given magnetic flux-surface is $d\phi/d\theta = q(\psi)$. In other words, the field-line appears as a straight-line in ϕ–θ space. Hence, ψ, θ, ϕ are often referred to as *straight field-line coordinates*.

It is convenient to define a flux-surface label, r, that can be interpreted as the mean minor radius of a given magnetic flux-surface. Thus, in its normalized form, r is the mean inverse aspect-ratio of the flux-surface. Writing $d\psi/dr = f(r)$, we get

$$\mathbf{B} = f\,\nabla\phi \times \nabla r + \frac{f\,q\,R^2}{\mathcal{J}}\,\nabla\phi, \tag{2}$$

where $\mathcal{J} = (\nabla r \times \nabla\theta \cdot \nabla\phi)^{-1}$ is the Jacobian of the r, θ, ϕ coordinate system. Making the specific choice, [17,18]

$$\mathcal{J}(r,\theta) \equiv (\nabla r \times \nabla\theta \cdot \nabla\phi)^{-1} \equiv R\left(\frac{\partial R}{\partial \theta}\frac{\partial Z}{\partial r} - \frac{\partial R}{\partial r}\frac{\partial Z}{\partial \theta}\right) = r\,R^2, \tag{3}$$

we obtain

$$\mathbf{B}(r,\theta) = f(r)\,\nabla\phi \times \nabla r + g(r)\,\nabla\phi, \tag{4}$$

4

where

$$g(r) = \frac{f\,q}{r} \tag{5}$$

It is easily seen, from the previous two equations, that, in the cylindrical limit, r morphs into the cylindrical radial coordinate. Note that $r = r(R, Z)$ and $\theta = \theta(R, Z)$. The magnetic axis corresponds to $r = 0$. The plasma-vacuum interface corresponds to $r = a$. Thus, a can be interpreted as the mean inverse-aspect ratio of the plasma boundary. The inboard mid-plane corresponds to $\theta = 0$. We require $g = 1$ on the magnetic axis in order to ensure that the normalized toroidal magnetic field-strength at the axis is unity.

More details of the equilibrium are given in Sect. A 2. It is clear, from the analysis of this section, that $g' = 0$ and $P' = 0$ in the current-free vacuum region, $r > a$, surrounding the plasma. Here, $' \equiv d/dr$, and $P(r)$ is the equilibrium plasma pressure profile. Obviously, $P(r) = 0$ in the vacuum region. In this paper, we are specifically interested in realistic diffuse plasma equilibria. In such equilibria, we expect $g(r)$, $f(r)$, $q(r)$, and $P(r)$, and their first derivatives with respect to r, to all be continuous across the plasma-vacuum interface. The net result is that the equilibrium magnetic field is continuous across the interface [see Eqs. (A1)–(A3)], which implies that there is no unresolved equilibrium current sheet flowing on the plasma boundary. Of course, such a current sheet would be completely unphysical.

III.   GENERAL AXISYMMETRIC PLASMA PERTURBATION

A.   Axisymmetric Ideal-MHD P.D.E.s

Let us assume that all perturbed quantities are independent of the toroidal angle, ϕ, and vary in time as $\exp(\gamma\,t)$. The perturbed plasma equilibrium satisfies the linearized, marginally-stable, ideal-MHD equations [18–20]

$$\mathbf{b} = \nabla \times (\boldsymbol{\xi} \times \mathbf{B}), \tag{6}$$

$$\nabla p = \mathbf{j} \times \mathbf{B} + \mathbf{J} \times \mathbf{b}, \tag{7}$$

$$\mathbf{j} = \nabla \times \mathbf{b}, \tag{8}$$

$$p = -\boldsymbol{\xi} \cdot \nabla P + \delta p, \tag{9}$$

$$\delta p = -\Gamma P \nabla \cdot \boldsymbol{\xi}, \tag{10}$$

where $\boldsymbol{\xi}(r, \theta)$ is the plasma displacement, $\mathbf{b}(r, \theta)$ the perturbed magnetic field, $\mathbf{j}(r, \theta)$ the perturbed current density, $p(r, \theta)$ the perturbed scalar pressure, and $\Gamma = 5/3$ the ratio of specific heats. Here, we are neglecting plasma inertia on the assumption that the wall slows the growth-time of the perturbation such that it is much longer than the Alfvén time.

In Sect. A 3, using the previous five equations as a starting point, we derive the following set of coupled partial differential equations (p.d.e.s) that govern the perturbed equilibrium, and which we shall refer to as the *axisymmetric ideal-MHD p.d.e.s*:

$$r \frac{\partial y}{\partial r} = \frac{\mathcal{Z}}{|\nabla r|^2} - \frac{r \, \nabla r \cdot \nabla \theta}{|\nabla r|^2} \frac{\partial y}{\partial \theta}, \tag{11}$$

$$r \frac{\partial \mathcal{Z}}{\partial r} = - \left[(\alpha_f \, \alpha_p + r \, \alpha_p')R^2 + q \, r \, \alpha_g' + r^2 \, \alpha_g^2 \right] y - \frac{\partial}{\partial \theta} \left(\frac{1}{|\nabla r|^2 \, R^2} \frac{\partial y}{\partial \theta} \right)$$

$$- \frac{\partial}{\partial \theta} \left(\frac{r \, \nabla r \cdot \nabla \theta}{|\nabla r|^2} \mathcal{Z} \right), \tag{12}$$

Here, $y(r, \theta) = f \, \boldsymbol{\xi} \cdot \nabla r$, $\mathcal{Z}(r, \theta) = -\mathbf{b} \cdot \mathcal{J} \, \nabla \phi \times \nabla r$, and $\alpha_g(r)$, $\alpha_p(r)$, and $\alpha_f(r)$ are defined in Eqs. (A34), (A55), and (A56), respectively. Note that the axisymmetric analysis of Sect. A 3 diverges from from the non-axisymmetric analysis of Ref. 11 at a fairly early stage.

B. Axisymmetric Ideal-MHD O.D.E.s

Let

$$y(r, \theta) = \sum_m y_m(r) \, e^{i m \theta}, \tag{13}$$

$$\mathcal{Z}(r, \theta) = \sum_m Z_m(r) \, e^{i m \theta}. \tag{14}$$

Here, the m are the set of (integer, but not necessarily positive) poloidal mode numbers included in the calculation. Equations (11) and (12) yield the *axisymmetric ideal-MHD ordinary differential equations (o.d.e.s)*:

$$r \frac{dy_m}{dr} = \sum_{m'} \left(A_m^{m'} \, Z_{m'} + B_m^{m'} \, y_{m'} \right), \tag{15}$$

6

$$r \frac{dZ_m}{dr} = \sum_{m'} \left(C_m^{m'} Z_{m'} + D_m^{m'} y_{m'} \right). \tag{16}$$

The coupling coefficients, $A_m^{m'}(r)$, $B_m^{m'}(r)$, $C_m^{m'}(r)$, and $D_m^{m'}(r)$ are specified in Sect. A 4. It is easily seen that $Z_0(r)$ is independent of r in the vacuum region, $r > a$, in which $\alpha_g = \alpha_p = 0$.

The axisymmetric ideal-MHD o.d.e.s play the same role for axisymmetric perturbations that the outer-region o.d.e.s, (102) and (103) of Ref. 11, play for non-axisymmetric perturbations. The main difference is that there are no singularities in the axisymmetric ideal-MHD o.d.e.s because an axisymmetric perturbation does not resonate with the plasma. In other words, there are no equilibrium magnetic flux-surfaces in the plasma at which $\mathbf{k} \cdot \mathbf{B} = 0$, where $\mathbf{k}$ is the wavevector of the perturbation. This is because $|\mathbf{B} \cdot \nabla \theta| > 0$ throughout a conventional tokamak plasma equilibrium.

C.   Properties of Axisymmetric Ideal-MHD O.D.E.s

In Sect. A 4, it is demonstrated that $A_{m'}^m = A_{m'}^{m*}$, $B_{m'}^m = -C_{m'}^{m*}$ $C_{m'}^m = -B_{m'}^{m*}$, $D_{m'}^m = D_{m'}^{m*}$. It follows from Eqs. (15) and (16) that

$$r \frac{d}{dr} \left[\sum_m (Z_m \, y_m^* - y_m \, Z_m^*) \right] = 0. \tag{17}$$

As we shall see in Sect. III G, the previous equation implies that the net electromagnetic energy flux across magnetic flux-surfaces is independent of r.

D.   Plasma Incompressibility

It is well known that the most unstable ideal perturbation to which a plasma equilibrium is subject does not compress the plasma. In other words, the perturbation is characterized by $\nabla \cdot \boldsymbol{\xi} = 0$.[20] In fact, the axisymmetric ideal-MHD o.d.e.s, (11) and (12), were derived on the assumption that $\nabla \cdot \boldsymbol{\xi} = 0$. (See Sect. A 3.) However, we must now ask whether it is possible to find a physical $\boldsymbol{\xi}(r, \theta)$ that is compatible with $\nabla \cdot \boldsymbol{\xi} = 0$. In Sect. A 3, it is shown that this is possible provided

$$\oint y(r, \theta) \frac{d\theta}{2\pi} = \oint R^2(r, \theta) \, y(r, \theta) \frac{d\theta}{2\pi} = 0 \tag{18}$$

7

for $0 \leq r \leq a$.

Now, in an up-down symmetric plasma equilibrium, the coupling coefficients, $A_m^{m'}(r)$, $B_m^{m'}(r)$, $C_m^{m'}(r)$, and $D_m^{m'}(r)$, are all real. [See Eqs. (109)–(120).] In this case, there are two independent classes of solutions to the axisymmetric ideal-MHD o.d.e.s, (13) and (14). The first class of solutions is such that

$$y(r, \theta) = \sum_{m>0} y_m(r) \, \sin(m\,\theta), \tag{19}$$

$$Z(r, \theta) = \sum_{m>0} Z_m(r) \, \sin(m\,\theta). \tag{20}$$

We shall refer to these solutions as *vertical modes*, because they give rise to predominately vertical plasma displacements. The second class of solutions is such that

$$y(r, \theta) = \sum_{m\geq0} y_m(r) \, \cos(m\,\theta), \tag{21}$$

$$Z(r, \theta) = \sum_{m\geq0} Z_m(r) \, \cos(m\,\theta). \tag{22}$$

We shall refer to these solutions as *horizontal modes*, because they give rise to predominately horizontal plasma displacements. It is clear from Eq. (18), given that $R(r, \theta)$ is even in θ [see Eq. (A83)], that vertical modes do not compress the plasma, whereas horizontal modes do compress the plasma.[21]

In conclusion, if we restrict our attention to vertical modes in up-down symmetric plasma equilibria then it is mathematically consistent to set $\nabla \cdot \boldsymbol{\xi} = 0$, which implies that our vertical modes are maximally unstable. We expect horizontal modes to be stable in a realistic vertically elongated plasma equilibrium,[21] so the exclusion of such modes from our consideration is not a serious drawback. Note that our vertical modes are not necessarily associated with pure up-down symmetric vertical motion (because they contain Fourier harmonics other than $m = 1$).[22]

E. Perturbed Electric Field

Let $\mathbf{e}$ be the perturbed electric field, which satisfies

$$\nabla \times \mathbf{e} = -\gamma\, \mathbf{b}. \tag{23}$$

8

Hence,

$$e_\phi = -\gamma\, y, \tag{24}$$

and

$$\frac{\partial e_\theta}{\partial r} - \frac{\partial e_r}{\partial \theta} = \gamma\, r\, \alpha_g\, y, \tag{25}$$

where use has been made of Eqs. (A20), (A21), (A50), and (A62). We also expect $\nabla \cdot \mathbf{e} = 0$, which implies that $e_r = e_\theta = 0$ in the vacuum region, $r \geq a$, in which $\alpha_g = 0$.

F. Toroidal Electromagnetic Torque

The net toroidal electromagnetic torque exerted on the region of the plasma lying within the magnetic flux-surface whose label is r is [11]

$$T_\phi(r) = \oint \oint r\, R^2\, b_\phi\, b^r\, d\theta\, d\phi. \tag{26}$$

It follows from Eqs. (A20) and (A39) that

$$T_\phi(r) = -\frac{\pi\, \alpha_g}{2} \oint \left(y^* \frac{\partial y}{\partial \theta} + y\, \frac{\partial y^*}{\partial \theta} \right) d\theta = -\frac{\pi\, \alpha_g}{2} \oint \frac{\partial |y|^2}{\partial \theta}\, d\theta = 0. \tag{27}$$

We conclude, not surprisingly, that an axisymmetric perturbation is incapable of exerting a net toroidal electromagnetic torque on the plasma.

In Ref. 12, the conservation of toroidal angular momentum is used to prove that the plasma and vacuum perturbed potential energy matrices are Hermitian. The fact that the toroidal electromagnetic torque is identically zero in the axisymmetric case negates this proof. Hence, we need to find a new conserved quantity that is not identically zero. The electromagnetic energy flux is found to play this role.

G. Electromagnetic Energy Flux

The net flux of electromagnetic energy across the plasma-vacuum interface is

$$\mathcal{E}(a) = \left[\oint \oint (\mathbf{e} \times \mathbf{b}) \cdot \nabla r\, \mathcal{J}\, d\theta\, d\phi \right]_{r=a} = \left[\oint \oint (e_\theta\, b_\phi - e_\phi\, b_\theta)\, d\theta\, d\phi \right]_{r=a}$$

9

$$= -\frac{\pi\,\gamma}{2} \oint (y\,\mathcal{Z}^* - y^*\,\mathcal{Z})_{r=a}\,d\theta = -\pi^2\,\gamma \sum_m (Z_m^*\,y_m - y_m^*\,Z_m)_{r=a}. \tag{28}$$

Here, use has been made of Eqs. (A49), (13), (14), and (24), as well as the fact that $e_\theta = 0$ for $r \geq a$. Now, Eq. (17) implies that $\sum_m(Z_m^*\,y_m - y_m^*\,Z_m)$ is independent of r. However, we expect $\sum_m(Z_m^*\,y_m - y_m^*\,Z_m) = 0$ for a well-behaved solution of the axisymmetric ideal-MHD o.d.e.s close to the magnetic axis $(r = 0)$. [See Eqs. (126) and (127).] Hence, we deduce that

$$\mathcal{E}(a) = 0. \tag{29}$$

In other words, the net flux of electromagnetic energy out of the plasma is zero.

H.   Perturbed Plasma Potential Energy

The perturbed plasma potential energy in the region of the plasma lying within the magnetic flux-surface whose label is r is [12,20]

$$\delta W_p(r) = \frac{1}{2} \oint \oint r\,R^2\,\xi^{r*}(-\mathbf{B}\cdot\mathbf{b} + \xi^r\,P')\,d\theta\,d\phi. \tag{30}$$

Here, we have neglected the contribution to the perturbed energy from plasma compressibility because $\nabla\cdot\boldsymbol{\xi} = 0$. (See Sect. III D.) However,

$$\mathbf{B}\cdot\mathbf{b} - \xi^r\,P' = B^\theta\,b_\theta + B^\phi\,b_\phi - \xi^r\,P' = -\frac{f}{r\,R^2}\left(\mathcal{Z} + q\,\alpha_g\,y + \alpha_p\,R^2\right), \tag{31}$$

where use has been made of Eqs. (5)–(A3), (A22), (A39), (A49), and (A55). Hence, we obtain

$$\delta W_p(r) = \frac{1}{2}\left[\oint\oint y^*\left(\mathcal{Z} + \alpha_g\,q\,y + \alpha_p\,R^2\,y\right)d\theta\,d\varphi\right]_r$$

$$= \pi^2\left[\sum_m y_m^*\left(Z_m + \alpha_g\,q\,y_m + \alpha_p \sum_{m'} a_m^{m'}\,y_m\right)\right]_r. \tag{32}$$

In particular, the net perturbed plasma potential energy is

$$\delta W_p(a) = \pi^2\left(\sum_m y_m^*\,Z_m\right)_a, \tag{33}$$

because $\alpha_g = \alpha_p = 0$ at $r = a$. However, it is clear from Equations (28) and (29) that $(\sum_m y_m^*\,Z_m)_a$ is real. Hence, we deduce that $\delta W_p(a)$ is real.

I. Perturbed Surface Potential Energy

In principle, there is a contribution to the perturbed potential energy from the plasma-vacuum interface. This contribution takes the form [20,23]

$$\delta W_s = \pi \oint_{r=a} \frac{|y^2|}{f^2 \, |\nabla r|^2} \, \nabla r \cdot \left[\!\!\left[\nabla r \left(P' + \frac{1}{2} \frac{\partial B^2}{\partial r} \right) \right]\!\!\right] \mathcal{J} \, d\theta, \tag{34}$$

where $[\!\![\cdots]\!\!] \equiv [\cdots]_{r=a-}^{r=a+}$. Here, we have made use of the fact that equilibrium force balance requires $P + B^2/2$ to be continuous across the plasma-vacuum interface.[20] However, in this paper we are only considering realistic diffuse plasma equilibria in which the pressure and current density are continuous across the interface. Such equilibria are characterized by $P'(a_-) = P'(a_+) = 0$, which implies that $[\!\![P']\!\!] = 0$. Moreover, it is clear from the large aspect-ratio analysis of Sect. A 5, that, as long as $q(r)$ and $s(r) \equiv r\, q'/q$ are continuous across the interface, and $g' = P' = 0$ on the interface, as is the case for the equilibria considered in this paper, then $[\!\![\partial B^2/\partial r]\!\!] = 0$.[24] We conclude that there is no contribution to the perturbed potential energy from the plasma-vacuum interface in a realistic diffuse plasma equilibrium. Indeed, such a contribution could only arise from an unresolved perturbed current sheet flowing around the plasma boundary. However, such a current sheet is clearly unphysical in a diffuse plasma equilibrium.

IV. GENERAL VACUUM SOLUTION

A. Introduction

In order to determine the growth-rate of the axisymmetric resistive wall mode, we need to calculate the total perturbed potential energy in two separate cases.[23,25] In the first case, the wall is treated as a perfect conductor. In the second, the wall is absent. Now, if the r, θ, ϕ coordinate system is extended into the vacuum region surrounding the plasma then, sufficiently far from the plasma, it eventually becomes singular. Thus, although the r, θ, ϕ coordinate system could be used to calculate the perfect-wall perturbed potential energy, provided that the wall is sufficiently close to the plasma, it cannot be used to calculate the no-wall perturbed potential energy. In order to calculate the latter energy, we need a coordinate

system that extends to infinity without becoming singular. Orthogonal toroidal coordinates, μ, η, ϕ, are the obvious choice. Note that toroidal coordinates are not flux coordinates. In other words, the plasma-vacuum interface does not correspond to a constant-μ surface. However, this is taken into account in our analysis.

B. Toroidal Coordinates

Let μ, η, ϕ be right-handed *orthogonal toroidal coordinates* defined such that [11,12,26]

$$R = \frac{\sinh \mu}{\cosh \mu - \cos \eta}, \tag{35}$$

$$Z = \frac{\sin \eta}{\cosh \mu - \cos \eta}. \tag{36}$$

The scale-factors of the toroidal coordinate system are

$$h_\mu = h_\eta = \frac{1}{\cosh \mu - \cos \eta} \equiv h, \tag{37}$$

$$h_\phi = \frac{\sinh \mu}{\cosh \mu - \cos \eta} = h \, \sinh \mu. \tag{38}$$

Moreover,

$$\mathcal{J}' \equiv (\nabla \mu \times \nabla \eta \cdot \nabla \phi)^{-1} = h^3 \, \sinh \mu. \tag{39}$$

C. Perturbed Magnetic Field

The curl-free perturbed magnetic field in the vacuum region is written $\mathbf{b} = \mathrm{i} \nabla V$, where $\nabla^2 V = 0$. The most general axisymmetric solution to Laplace's equation is [12,27]

$$V(z, \eta) = \sum_m (z - \cos \eta)^{1/2} \, U_m(z) \, \mathrm{e}^{-\mathrm{i} m \eta}, \tag{40}$$

$$U_m(z) = p_m \, \hat{P}_{|m|-1/2}(z) + q_m \, \hat{Q}_{|m|-1/2}(z), \tag{41}$$

where $z = \cosh \mu$, the p_m and q_m are arbitrary complex coefficients, and

$$\hat{P}_{|m|-1/2}(z) = \cos(|m| \, \pi) \frac{\sqrt{\pi} \, \Gamma(|m| + 1/2) \, a^{|m|}}{2^{|m|-1/2} \, |m|!} \, P_{|m|-1/2}(z), \tag{42}$$

12

$$\hat{Q}_{|m|-1/2}(z) = \cos(|m|\,\pi)\,\frac{2^{\,|m|-1/2}\,|m|!}{\sqrt{\pi}\,\Gamma(|m|+1/2)\,a^{\,|m|}}\,Q_{|m|-1/2}(z). \tag{43}$$

Here, the $P_{|m|-1/2}(z)$ and $Q_{|m|-1/2}(z)$ are toroidal functions,[28] and $\Gamma(z)$ is a gamma function.[29]

In the large-aspect ratio limit, $r \ll 1$, it can be demonstrated that [30]

$$z \simeq \frac{1}{r}, \tag{44}$$

$$z^{1/2}\,\hat{P}_{-1/2}(z) \simeq \frac{1}{2}\ln\left(\frac{8}{r}\right), \tag{45}$$

$$z^{1/2}\,\hat{P}_{|m|-1/2}(z) \simeq \frac{\cos(|m|\,\pi)\,(r/a)^{-|m|}}{|m|}, \tag{46}$$

$$z^{1/2}\,\hat{Q}_{|m|-1/2}(z) \simeq \frac{\cos(|m|\,\pi)\,(r/a)^{|m|}}{2}. \tag{47}$$

Note that Eq. (46) only applies to $m \neq 0$.

D.   Toroidal Electromagnetic Angular Momentum Flux

The outward flux of toroidal angular momentum across a constant-z surface is [11,12]

$$T_\phi(z) = -\oint\oint \mathcal{J}'\,b_\phi\,b^\mu\,d\eta\,d\phi = 0, \tag{48}$$

because $b_\phi = i\,\partial V/\partial \phi = 0$. Of course, the flux has to be zero because the flux of angular momentum across the plasma-vacuum interface is zero, and there are no sources of angular momentum in the vacuum region surrounding the plasma. (See Sect. III F.)

E.   Electromagnetic Energy Flux

The outward flux of electromagnetic energy flux across a surface of constant z is

$$\mathcal{E}(z) = -\oint\oint \mathcal{J}'\,\mathbf{e}\times\mathbf{b}\cdot\nabla\mu\,d\eta\,d\phi = -i\,\frac{\pi}{2}\oint\left(e_\phi\,\frac{\partial V^*}{\partial \eta} - e_\phi^*\,\frac{\partial V}{\partial \eta}\right)d\eta, \tag{49}$$

given that $e_\mu = e_\eta = 0$ in the vacuum. However, $\nabla\times\mathbf{e} = -\gamma\,\mathbf{b}$ implies that

$$\frac{\partial e_\phi}{\partial \eta} = -i\,\gamma\,h\,\sinh\mu\,\frac{\partial V}{\partial \mu} = -i\,\gamma\,h\,(z^2-1)\,\frac{\partial V}{\partial z}. \tag{50}$$

Thus,

$$\mathcal{E}(z) = \mathrm{i}\,\frac{\pi}{2}\oint\left(\frac{\partial e_\phi}{\partial\eta}\,V^* - \frac{\partial e_\phi^*}{\partial\eta}\,V\right)d\eta = \frac{\pi\,\gamma}{2}\oint h\,(z^2-1)\left(\frac{\partial V}{\partial z}\,V^* - \frac{\partial V^*}{\partial z}\,V\right)d\eta$$

$$= -\pi^2\,\gamma\sum_m(p_m\,q_m^* - q_m\,p_m^*)\,(z^2-1)\,\mathcal{W}(P_{|m|-1/2}, Q_{|m|-1/2}), \tag{51}$$

where we have integrated by parts, and $\mathcal{W}(f,g) \equiv f\,dg/dz - g\,df/dz$. However,[30]

$$\mathcal{W}(P_{|m|-1/2}, Q_{|m|-1/2}) = \frac{1}{1-z^2}, \tag{52}$$

so

$$\mathcal{E}(z) = \pi^2\,\gamma\sum_m(p_m\,q_m^* - q_m\,p_m^*). \tag{53}$$

Note that $\mathcal{E}(z)$ is independent of z, as must be the case because there are no energy sources in the vacuum region.

F. Solution in Vacuum Region

According to Eq. (A20) and (A49),

$$\frac{\partial y}{\partial\theta} = \mathcal{J}\,\mathbf{b}\cdot\nabla r = \mathrm{i}\,\mathcal{J}\,\nabla V\cdot\nabla r, \tag{54}$$

$$\mathcal{Z} = -\mathcal{J}\,\nabla\phi\times\nabla r\cdot\mathbf{b} = -\mathrm{i}\,\frac{\partial V}{\partial\theta}. \tag{55}$$

Now, we have already seen that $Z_0 \equiv \oint\mathcal{Z}\,d\theta/(2\pi) = 0$ is independent of r in the vacuum region. (See Sect. III B.) However, it is clear that Eq. (55) mandates that this constant value be zero. This constraint implies that the axisymmetric ideal modes to which the plasma equilibrium is subject do not change the net toroidal current flowing in the plasma. [See Eqs. (A49) and (121).] Note, further, that $y_0 \equiv \oint y\,d\theta/(2\pi)$ does not influence the vacuum potential, $V(r,\theta)$.

The previous two equations yield [12]

$$\underline{V}(r) = \underline{\underline{\mathcal{P}}}(r)\,\underline{p} + \underline{\underline{\mathcal{Q}}}(r)\,\underline{q}, \tag{56}$$

$$\underline{\psi}(r) = \underline{\underline{\mathcal{R}}}(r)\,\underline{p} + \underline{\underline{\mathcal{S}}}(r)\,\underline{q}, \tag{57}$$

14

where $V(r,\theta) = \sum_m V_m(r)\, e^{i\,m\,\theta}$, $Z_m(r) = m\, V_m(r)$, $\psi_m(r) = m\, y_m(r)$, $\underline{V}(r)$ is the vector of the $V_m(r)$ values, $\underline{\psi}(r)$ is the vector of the $\psi_m(r)$ values, $\underline{\underline{P}}(r)$ is the matrix of the

$$\mathcal{P}_{mm'}(r) = \oint_r (z - \cos\eta)^{1/2}\, \hat{P}_{|m'|-1/2}(z)\, \exp[-i\,(m\,\theta + m'\,\eta)]\, \frac{d\theta}{2\pi} \tag{58}$$

values, $\underline{\underline{Q}}(r)$ is the matrix of the

$$\mathcal{Q}_{mm'}(r) = \oint_r (z - \cos\eta)^{1/2}\, \hat{Q}_{|m'|-1/2}(z)\, \exp[-i\,(m\,\theta + m'\,\eta)]\, \frac{d\theta}{2\pi} \tag{59}$$

values, $\underline{\underline{R}}(r)$ is the matrix of the

$$
\begin{aligned}
\mathcal{R}_{mm'}(r) = \oint_r \Bigg\{ & \left[\frac{1}{2}\,(z - \cos\eta)^{-1/2}\, \hat{P}_{|m'|-1/2}(z) + (z - \cos\eta)^{1/2}\, \frac{d\hat{P}_{|m'|-1/2}}{dz} \right] \mathcal{J}\,\nabla r \cdot \nabla z \\
& + \left[\frac{1}{2}\,(z - \cos\eta)^{-1/2}\, \sin\eta - i\,m'\,(z - \cos\eta)^{1/2} \right] \hat{P}_{|m'|-1/2}(z)\, \mathcal{J}\,\nabla r \cdot \nabla\eta \Bigg\} \\
& \times \exp[-i\,(m\,\theta + m'\,\eta)]\, \frac{d\theta}{2\pi}
\end{aligned}
\tag{60}
$$

values, $\underline{\underline{S}}(r)$ is the matrix of the

$$
\begin{aligned}
\mathcal{S}_{mm'}(r) = \oint_r \Bigg\{ & \left[\frac{1}{2}\,(z - \cos\eta)^{-1/2}\, \hat{Q}_{|m'|-1/2}(z) + (z - \cos\eta)^{1/2}\, \frac{d\hat{Q}_{|m'|-1/2}}{dz} \right] \mathcal{J}\,\nabla r \cdot \nabla z \\
& + \left[\frac{1}{2}\,(z - \cos\eta)^{-1/2}\, \sin\eta - i\,m'\,(z - \cos\eta)^{1/2} \right] \hat{Q}_{|m'|-1/2}(z)\, \mathcal{J}\,\nabla r \cdot \nabla\eta \Bigg\} \\
& \times \exp[-i\,(m\,\theta + m'\,\eta)]\, \frac{d\theta}{2\pi}
\end{aligned}
\tag{61}
$$

values, $\underline{p}$ is the vector of the p_m coefficients, and $\underline{q}$ is the vector of the q_m coefficients. Here, the subscript r on the integrals indicates that they are taken at constant r.

G. Energy Conservation

By analogy with Eq. (28), the net flux of electromagnetic energy across a surface of constant r in the vacuum region is

$$\mathcal{E}(r) = -\pi^2\,\gamma\,(\underline{V}^\dagger\,\underline{\psi} - \underline{\psi}^\dagger\,\underline{V}). \tag{62}$$

15

However, energy conservation requires this flux to be equal to the energy flux through the vacuum region, so Eq. (53) gives

$$\mathcal{E}(r) = \pi^2 \, \gamma \, (\underline{q}^\dagger \, \underline{p} - \underline{p}^\dagger \, \underline{q}). \tag{63}$$

Equations (56), (57), and the previous two equations, yield [12]

$$\underline{\underline{\mathcal{P}}}^\dagger \, \underline{\underline{\mathcal{R}}} = \underline{\underline{\mathcal{R}}}^\dagger \, \underline{\underline{\mathcal{P}}}, \tag{64}$$

$$\underline{\underline{\mathcal{Q}}}^\dagger \, \underline{\underline{\mathcal{S}}} = \underline{\underline{\mathcal{S}}}^\dagger \, \underline{\underline{\mathcal{Q}}}, \tag{65}$$

$$\underline{\underline{\mathcal{P}}}^\dagger \, \underline{\underline{\mathcal{S}}} - \underline{\underline{\mathcal{R}}}^\dagger \, \underline{\underline{\mathcal{Q}}} = \underline{\underline{1}}. \tag{66}$$

It can also be demonstrated that

$$\underline{\underline{\mathcal{Q}}} \, \underline{\underline{\mathcal{P}}}^\dagger = \underline{\underline{\mathcal{P}}} \, \underline{\underline{\mathcal{Q}}}^\dagger, \tag{67}$$

$$\underline{\underline{\mathcal{R}}} \, \underline{\underline{\mathcal{S}}}^\dagger = \underline{\underline{\mathcal{S}}} \, \underline{\underline{\mathcal{R}}}^\dagger. \tag{68}$$

The previous five equations hold throughout the vacuum region. In fact, checking that these relations hold in the vacuum region constitutes a good numerical test that the matching between the r, θ, ϕ and the μ, η, ϕ coordinate systems is working correctly. These relations are found to hold to a good approximation in all of the calculations described in Sect. VIII.

H. No-Wall Matching Condition

Suppose that the plasma is surrounded by a vacuum region that extends to infinity. In this case,

$$\underline{q} = \underline{0}, \tag{69}$$

because the $\hat{Q}_{|m|-1/2}(z)$ functions blow up in an unphysical manner as $r/a \to \infty$. [See Eq. (47)]. It immediately follows from Eq. (63) that

$$\mathcal{E}(z) = 0. \tag{70}$$

In other words, as we would expect, there is zero net flux of electromagnetic energy through the vacuum, because we have already demonstrated that there is zero energy flux across the

plasma-vacuum interface. [See Equation (29).] Equations (56) and (57) imply that

$$\underline{V}(r = a_+) = \underline{\underline{H}} \, \underline{\psi}(r = a),$$ (71)

where

$$\underline{\underline{H}} = \underline{\underline{P}}_a \, \underline{\underline{R}}_a^{-1}$$ (72)

is termed the *no-wall vacuum matrix*. Here, $\underline{\underline{P}}_a = \underline{\underline{P}}(r = a)$, et cetera. Equation (64) ensures that $\underline{\underline{H}}$ is Hermitian.

I.   Perfect-Wall Matching Condition

Suppose that the plasma is surrounded by a vacuum region that is bounded by a perfectly conducting wall that is conformal to the plasma-vacuum interface, and whose inner surface lies at $r = b_w \, a$, where $b_w \geq 1$. Because the wall is perfectly conducting, $\underline{\psi}(r = b_w \, a) = \underline{0}$.[20] In other words, the normal component of the perturbed magnetic field is zero at the inner surface of the wall. It follows from Eq. (57) that

$$\underline{p} = -\underline{\underline{I}}_b \, \underline{q},$$ (73)

where

$$\underline{\underline{I}}_b = \underline{\underline{R}}_b^{-1} \, \underline{\underline{S}}_b$$ (74)

is termed the *wall matrix*. Here, $\underline{\underline{R}}_b = \underline{\underline{R}}(r = b_w \, a)$, et cetera. Equation (68) ensures that $\underline{\underline{I}}_b$ is Hermitian. It immediately follows from Eq. (63) that

$$\mathcal{E}(z) = 0.$$ (75)

In other words, as we would again expect, there is zero net flux of electromagnetic energy through the vacuum, because we have already demonstrated that there is zero energy flux across the plasma-vacuum interface. [See Equation (29).]

Making use of Eqs. (56) and (57), the matching condition at the plasma-vacuum interface for a perfectly-conducting wall becomes

$$\underline{V}(r = a_+) = \underline{\underline{G}} \, \underline{\psi}(r = a),$$ (76)

17

where

$$\underline{\underline{G}} = (\underline{\underline{Q}}_a - \underline{\underline{P}}_a \underline{\underline{I}}_b)(\underline{\underline{S}}_a - \underline{\underline{R}}_a \underline{\underline{I}}_b)^{-1} \tag{77}$$

is termed the *perfect-wall vacuum matrix.* It is easily demonstrated from Eqs. (64)–(66) that

$$\underline{\underline{G}} - \underline{\underline{G}}^\dagger = -[(\underline{\underline{S}}_a - \underline{\underline{R}}_a \underline{\underline{I}}_b)^{-1}]^\dagger (\underline{\underline{I}}_b - \underline{\underline{I}}_b^\dagger)(\underline{\underline{S}}_a - \underline{\underline{R}}_a \underline{\underline{I}}_b)^{-1}. \tag{78}$$

Thus, the perfect-wall vacuum matrix, $\underline{\underline{G}}$, is Hermitian because the wall matrix, $\underline{\underline{I}}_b$, is Hermitian.

J.   Perturbed Vacuum Potential Energy

Equation (A20) implies that

$$\mathcal{J}\,\nabla r \cdot \nabla V = -\mathrm{i}\,\frac{\partial y}{\partial \theta}. \tag{79}$$

The perturbed potential energy in the vacuum region is [12,20]

$$
\begin{aligned}
\delta W_v &= \frac{1}{2}\int_{a_+}^{\infty} \oint \oint \mathbf{b}^* \cdot \mathbf{b}\, \mathcal{J}\, dr\, d\theta\, d\phi = \frac{1}{2}\int_{a_+}^{\infty} \oint \oint \nabla V^* \cdot \nabla V\, \mathcal{J}\, dr\, d\theta\, d\phi \\
&= -\frac{1}{2}\left(\oint \oint \mathcal{J}\,\nabla r \cdot \nabla V^* \, V\, d\theta\, d\phi\right)_{a_+} = -\frac{1}{2}\left[\oint \oint \left(-\mathrm{i}\frac{\partial y}{\partial \theta}\right)^* V\, d\theta\, d\phi\right]_{a_+} \\
&= -\pi^2 \left(\sum_m m\, y_m^*\, V_m\right)_{a_+},
\end{aligned}
\tag{80}
$$

where use has been made of the facts that $\nabla^2 V = 0$, and $V = 0$ at infinity in the no-wall case, and $\nabla r \cdot \nabla V = 0$ at the ideal wall in the perfect-wall case.

V.   GENERAL IDEAL STABILITY

A.   Perturbed Plasma Potential Energy Matrix

Suppose that the poloidal harmonics included in the calculation range from $m = -m_{\max}$ to $m = m_{\max}$, where $m_{\max} > 0$. Let the $y_{mm'}(r)$ and the $Z_{mm'}(r)$ be linearly independent solutions of the axisymmetric ideal-MHD o.d.e.s, (15) and (16), that are well-behaved at the

18

magnetic axis. Here, m indexes the poloidal harmonic, whereas m' indexes the dominant poloidal harmonic close to the magnetic axis. (See Sect. VII F.) We can form $J = 2\,m_{\mathrm{max}}$ linearly independent solutions that all have $Z_0 = 0$ at $r = a$, as mandated by the matching condition (55). Let these new solutions be denoted the $\hat{y}_{mj}(r)$ and the $\hat{Z}_{mj}(r)$, where j runs from 1 to J. The most general solution to the axisymmetric ideal-MHD o.d.e.s that satisfies the constraint $Z_0(a) = 0$ is written

$$y_m(r) = \sum_{j=1,J} \hat{y}_{mj}(r)\,\alpha_j, \tag{81}$$

$$Z_m(r) = \sum_{j=1,J} \hat{Z}_{mj}(r)\,\alpha_j, \tag{82}$$

where the α_j are arbitrary complex coefficients. Here, m indexes the poloidal harmonic and j indexes the solution.

According to Eq. (32), the net perturbed plasma potential energy is

$$\delta W_p(a) = \pi^2\,\underline{y}^\dagger\,\underline{Z}, \tag{83}$$

where $\underline{y}$ is the vector of the $y_m(a)$ values, excluding the $m = 0$ harmonic, and $\underline{Z}$ the vector of the $Z_m(a_-)$ values, excluding the $m = 0$ harmonic. We can exclude the $m = 0$ harmonic because, by construction, our solutions are such that $Z_0(a_-) = 0$. It follows that

$$\delta W_p(a) = \pi^2\,\underline{\alpha}^\dagger\,\underline{\underline{y}}^\dagger\,\underline{\underline{Z}}\,\underline{\alpha}, \tag{84}$$

where $\underline{\alpha}$ is the vector of the α_j values, $\underline{\underline{y}}$ the matrix of the $\hat{y}_{mj}(a)$ values, excluding the $m = 0$ harmonic, and $\underline{\underline{Z}}$ the matrix of the $\hat{Z}_{mj}(a_-)$ values, excluding the $m = 0$ harmonic. If

$$\underline{\underline{\chi}} = \underline{\underline{W}}_p\,\underline{\underline{y}}. \tag{85}$$

then

$$\delta W_p(a) = \pi^2\,\underline{\alpha}^\dagger\,\underline{\underline{y}}^\dagger\,\underline{\underline{W}}_p\,\underline{\underline{y}}\,\underline{\alpha}. \tag{86}$$

We have already shown that $\delta W_p(a)$ is real, which implies that $\underline{\underline{W}}_p$, which is known as the *perturbed plasma potential energy matrix*, is Hermitian.

19

B. Perturbed Vacuum Potential Energy Matrix

According to Eq. (80), the perturbed vacuum potential energy is

$$\delta W_v = -\pi^2 \sum_m m\, y_m^*(a)\, V_m(a_+),$$ (87)

excluding the $m = 0$ harmonic, which obviously does not affect the vacuum energy. However, Eqs. (71) and (76) imply that

$$V_m(a_+) = \sum_{m'} H_{mm'}\, m'\, y_{m'}(a)$$ (88)

in the no-wall case, and

$$V_m(a_+) = \sum_{m'} G_{mm'}\, m'\, y_{m'}(a)$$ (89)

in the perfect-wall case. Here, we have excluded the $m' = 0$ harmonic, which also obviously does not affect the vacuum energy. Hence, we can write

$$\delta W_v = \pi^2\, \underline{y}^\dagger\, \underline{\underline{W}}_v\, \underline{y},$$ (90)

where $\underline{\underline{W}}_v$ is the matrix of the $-m\, H_{mm'}\, m'$ values in the no-wall case, excluding the $m = 0$ and $m' = 0$ harmonics, and the $-m\, G_{mm'}\, m'$ values in the perfect-wall case, likewise excluding the $m = 0$ and $m' = 0$ harmonics,. Given that $H_{mm'}$ and $G_{mm'}$ are Hermitian, we deduce that $\underline{\underline{W}}_v$, which is known as the *perturbed vacuum potential energy matrix*, is Hermitian. It follows that

$$\delta W_v = \pi^2\, \underline{\alpha}^\dagger\, \underline{y}^\dagger\, \underline{\underline{W}}_v\, \underline{y}\, \underline{\alpha}.$$ (91)

C. Total Perturbed Potential Energy Matrix

The total perturbed potential energy is

$$\delta W = \delta W_p(a) + \delta W_v = \pi^2\, \underline{\alpha}^\dagger\, \underline{y}^\dagger\, \underline{\underline{W}}\, \underline{y}\, \underline{\alpha},$$ (92)

where

$$\underline{\underline{W}} = \underline{\underline{W}}_p + \underline{\underline{W}}_v.$$ (93)

Given that $\underline{\underline{W}}_p$ and $\underline{\underline{W}}_v$ are both Hermitian, we deduce that $\underline{\underline{W}}$, which is known as the *total perturbed potential energy matrix*, is Hermitian.

D. Ideal Stability

The fact that $\underline{\underline{W}}$ is Hermitian allows us to write

$$\underline{\underline{W}}\,\underline{\underline{\beta}} = \underline{\underline{\beta}}\,\underline{\underline{\Lambda}}, \tag{94}$$

$$\underline{\underline{\beta}}^\dagger\,\underline{\underline{\beta}} = \underline{\underline{1}}, \tag{95}$$

where $\underline{\underline{\beta}}$ is real, and $\underline{\underline{\Lambda}}$ is the diagonal matrix of the real λ_m values. If $\underline{\hat{\alpha}} = \underline{\underline{\beta}}^\dagger\,\underline{\underline{y}}\,\underline{\alpha}$ then

$$\delta W = \pi^2\,\underline{\hat{\alpha}}^\dagger\,\underline{\underline{\Lambda}}\,\underline{\hat{\alpha}} = \pi^2 \sum_{m=1,J} |\hat{\alpha}_m|^2\,\lambda_m. \tag{96}$$

Thus, if any of the λ_m are negative then solutions exist for which δW is negative, and the plasma is consequently unstable to an axisymmetric ideal mode.[20]

Suppose that $\sum_m |\hat{\alpha}_m|^2 = 1$. The ideal energy of the mth mode, for which $\hat{\alpha}_{m'} = \delta_{mm'}$, is

$$\delta W_m = \pi^2\,\lambda_m. \tag{97}$$

However,

$$\underline{\underline{\Lambda}} = \underline{\underline{\beta}}^\dagger\,\underline{\underline{W}}\,\underline{\underline{\beta}}, \tag{98}$$

Thus, the diagonal components of $\underline{\underline{\beta}}^\dagger\,\underline{\underline{W}}_p\,\underline{\underline{\beta}}$ and $\underline{\underline{\beta}}^\dagger\,\underline{\underline{W}}_v\,\underline{\underline{\beta}}$ are the plasma and vacuum contributions to the λ_m, respectively. The eigenfunction of the mth mode is conveniently normalized such that $y_{m'}(a) = \beta_{m'm}$.

VI. GENERAL RESISTIVE WALL MODE STABILITY

The unnormalized mean minor radius of the wall is $b = b_w\,\bar{a}$, where $\bar{a} = \epsilon\,R_0$ is the unnormalized mean minor radius of the plasma. Suppose that the wall is resistive, and possesses an (unnormalized) electrical conductivity σ_w, as well as an (unnormalized) uniform radial thickness d. Consider a particular axisymmetric ideal mode for which the total perturbed potential energy in the absence of a wall, δW_{nw}, is negative, but the total perturbed potential energy in the presence of a perfectly conducting wall, δW_{pw}, is positive. In this case, the no-wall ideal mode is unstable (because $\delta W_{nw} < 0$). In the absence of the wall, this mode would

grow very rapidly on an Alfvénic timescale. On the other hand, the mode is completely stabilized if the wall is perfectly conducting (because $\delta W_{pw} > 0$). However, because the wall is not perfectly conducting, the unstable ideal mode is instead converted into a much more slowly growing *resistive wall mode.*

Let the (unnormalized) growth-rate of the resistive wall mode be

$$\gamma = \frac{\hat{\gamma}}{\tau_w}, \tag{99}$$

where

$$\tau_w = \mu_0 \, \sigma_w \, b \, d \tag{100}$$

is the (unnormalized) L/R time of the wall. (See Sect. A 1.)   The normalized growth-rate of the resistive wall mode is specified by [23,25]

$$\sqrt{\frac{\hat{\gamma}}{\delta_w}} \tanh\left(\sqrt{\delta_w \, \hat{\gamma}}\right) = -\frac{\delta W_{nw}}{\alpha_w \, \delta W_{pw}}, \tag{101}$$

where $\delta_w = d/b$, and

$$\alpha_w = \frac{(1/2) \int |\mathbf{A}_{nw} \times \mathbf{n}_w|^2 \, dS_w}{\epsilon \, b_w \, (\delta W_{v\,pw} - \delta W_{v\,nw})}. \tag{102}$$

Here, $\delta W_{v\,nw}$ is the vacuum potential energy in the absence of a wall, whereas $\delta W_{n\,pw}$ is the vacuum energy in the presence of a perfectly conducting wall. Moreover, dS_w is an element of the inner surface of the wall, and the integral is over the whole inner surface. Furthermore, the perturbed magnetic field in the vacuum region, in the no-wall case, is written $\nabla \times \mathbf{A}_{nw}$. It is easily demonstrated from Eqs. (A20) and (A21) that $\mathbf{A}_{nw} = \sum_m y_{m\,nw}(r) \, e^{i\,m\,\theta} \, \nabla\phi$, where the $y_{m\,nw}(r)$ are the y-components of the no-wall eigenfunction of the mode in question. Here, we have made use of the fact that $b^\phi = 0$ in the vacuum region, because $\alpha_g = 0$. [See Eqs. (A50) and (A62).] Finally, $dS_w = \mathcal{J} \, d\theta \, d\phi$. Hence, we deduce that

$$\alpha_w = \frac{\pi^2 \left(\sum_{m \neq 0} |y_{m\,nw}|^2\right)_{\hat{r}=b_w}}{\delta W_{v\,pw} - \delta W_{v\,nw}}. \tag{103}$$

Here, we have neglected $y_{0\,nw}$ because y_0 does not affect the vacuum energy. (See Sect. V A.)

The *wall parameter,* α_w, is sometimes expressed as $\alpha_w = b_{\text{eff}}/b$, where b_{eff} is the "effective" mean minor radius of the wall.[25] In the cylindrical limit,

$$\alpha_w = \frac{1}{2\,|m|} \left[1 - \left(\frac{\bar{a}}{b}\right)^{2\,|m|}\right]. \tag{104}$$

In fact, $1/\alpha_w$ measures the strength of the inductive coupling between the wall and the plasma.

Given that $\underline{q} = \underline{0}$ for a no-wall solution, Eq. (57) yields

$$\underline{\underline{m}}\,\underline{y}_b = \underline{\underline{\mathcal{R}}}_b\,\underline{\underline{\mathcal{R}}}_a^{-1}\,\underline{\underline{m}}\,\underline{y}_a, \tag{105}$$

which enables us to determine the $y_{m \neq 0\,nw}(\hat{r} = b_w)$ from the $y_{m \neq 0\,nw}(\hat{r} = 1)$. Here, $\underline{\underline{m}}$ is the diagonal matrix of the poloidal mode numbers.

Finally, in the *thin-wall* limit, $\delta_w \ll 1$, Eq. (101) simplifies to give

$$\hat{\gamma} = -\frac{\delta W_{nw}}{\alpha_w\,\delta W_{pw}}. \tag{106}$$

VII.   INVERSE ASPECT-RATIO EXPANDED TOKAMAK EQUILIBRIUM

A.   Introduction

Up to now, our analysis has been completely general. At this stage, we introduce the simplifying approximation of an inverse aspect-ratio expanded plasma equilibrium. However, as discussed in Sect. III D, we must restrict our discussion to up-down symmetric equilibria in order to ensure that $\nabla \cdot \boldsymbol{\xi} = 0$.

B.   Equilibrium Magnetic Flux-Surfaces

Let us assume that the inverse aspect-ratio of the plasma, $\epsilon = a/R_0 = a$ (since R_0 is normalized to unity), is such that $0 < \epsilon \ll 1$. Let $r = \epsilon\,\hat{r}$, $\nabla = \epsilon^{-1}\,\hat{\nabla}$, and $' \to \epsilon^{-1}\,'$. Suppose that the loci of the up-down symmetric equilibrium magnetic flux-surfaces can be written in the parametric form:[11,12,18]

$$R(\hat{r}, \omega) = 1 - \epsilon\,\hat{r}\,\cos\omega + \epsilon^2 \sum_{j>0} H_j(\hat{r})\,\cos[(j-1)\,\omega] + \epsilon^3\,L(\hat{r})\,\cos\omega, \tag{107}$$

$$Z(\hat{r}, \omega) = \epsilon\,\hat{r}\,\sin\omega + \epsilon^2 \sum_{j>1} H_j(\hat{r})\,\sin[(j-1)\,\omega] - \epsilon^3\,L(\hat{r})\,\sin\omega, \tag{108}$$

where j is a positive integer. Here, $H_1(\hat{r})$ controls the relative horizontal locations of the flux-surface centroids, $H_2(\hat{r})$ controls the the flux-surface elongation, $H_3(\hat{r})$ controls the flux-surface triangularity, et cetera, whereas $L(\hat{r})$ is a flux-surface re-labelling parameter. Moreover, $\omega(R,Z)$ is a geometric poloidal angle that is distinct from the straight poloidal angle $\theta(R,Z)$. (The relationship between these two angles is specified in Sect. A 5 a.)

C.   Coupling Coeffiecients

In Sect. A 5, the following expressions for the coupling coefficients that appear in the axisymmetric ideal-MHD o.d.e.s, (15) and (16), are derived:

$$A_m^m(\hat{r}) = 1 + \epsilon^2 \left(-\frac{3\,\hat{r}^{\,2}}{4} + H_1 + S_1 \right), \tag{109}$$

$$A_m^{m\pm1}(\hat{r}) = -\epsilon\, H_1', \tag{110}$$

$$A_m^{m\pm j}(\hat{r}) = -\epsilon\, H_j' \qquad \text{for } j > 1, \tag{111}$$

$$B_m^m(\hat{r}) = 0, \tag{112}$$

$$B_m^{m\pm1}(\hat{r}) = \pm\epsilon\,(m\pm1)\left[\hat{r} - p_2'\,q^2 + (1-s)\,H_1'\right], \tag{113}$$

$$B_m^{m\pm j}(\hat{r}) = \pm\epsilon\,\frac{m\pm j}{j}\left[(1-s)\,H_j' - (j^2-1)\,\frac{H_j}{\hat{r}}\right] \qquad \text{for } j > 1, \tag{114}$$

$$C_m^m(\hat{r}) = 0, \tag{115}$$

$$C_m^{m\pm1}(\hat{r}) = \pm\epsilon\,m\left[\hat{r} - p_2'\,q^2 + (1-s)\,H_1'\right], \tag{116}$$

$$C_m^{m\pm j}(\hat{r}) = \pm\epsilon\,\frac{m}{j}\left[(1-s)\,H_j' - (j^2-1)\,\frac{H_j}{\hat{r}}\right] \qquad \text{for } j > 1, \tag{117}$$

$$
\begin{aligned}
D_m^m(\hat{r}) = {}& m^2 + q\,\hat{r}\,\frac{d}{d\hat{r}}\left(\frac{2-s}{q}\right) + \epsilon^2\,m^2\,S_4 \\
& + \epsilon^2\left\{ -\hat{r}^{\,2}\left(\frac{2-s}{q}\right)^2 + q\,\hat{r}\,\frac{d\Sigma}{d\hat{r}} - \hat{r}\,\frac{d}{d\hat{r}}(\hat{r}\,p_2') - 2\,(1-s)\,\hat{r}\,p_2' \right. \\
& \left. + 2\,\hat{r}\,p_2'\,q^2\left(-2 + \frac{3\,p_2'\,q^2}{\hat{r}}\right) + 2\,H_1'\,q^2\left[\frac{d}{d\hat{r}}(\hat{r}\,p_2') - 4\,(1-s)\,p_2'\right]\right\},
\end{aligned}
\tag{118}
$$

$$D_m^{m\pm1}(\hat{r}) = \epsilon\,q^2\left[\frac{d}{d\hat{r}}(\hat{r}\,p_2') - (2-s)\,p_2'\right] + \epsilon\,m\,(m\pm1)\,(\hat{r} - H_1'), \tag{119}$$

$$D_m^{m\pm j}(\hat{r}) = -\epsilon\, m\,(m\pm j)\, H_j' \quad \text{for } j > 1. \tag{120}$$

Here, p_2, Σ, and S_4 are defined in Eqs. (A86), and (A91)–(A95). Our system of equations is now complete.

D. Toroidal Plasma Current

The net toroidal plasma current flowing in the plasma is given by

$$I_p = \oint_{r=a} \mathcal{J}\,\nabla\phi \times \nabla r \cdot \mathbf{B}\, d\theta = \oint_{r=a} B_\theta\, d\theta, \tag{121}$$

which yields

$$I_p = \gamma_{\text{shape}}\, I_{p\,\text{cly}}, \tag{122}$$

where

$$I_{p\,\text{cyl}} = \frac{2\pi\, a^2\, g(a)}{q(a)} \tag{123}$$

is the plasma current predicted by cylindrical theory, whereas

$$\gamma_{\text{shape}} = \langle |\hat{\nabla}\hat{r}|^2 \rangle_{\hat{r}=1} \tag{124}$$

is the factor by which the toroidal current is increased due to the shaping of the plasma's poloidal boundary.

E. Plasma Self-Inductance

The dimensionless self-inductance of the plasma is conventionally defined as [11]

$$l_i = \frac{2\int_0^1 \hat{r}\, f^2\, \langle |\hat{\nabla}\hat{r}|^2 \rangle\, d\hat{r}}{(f\, \langle |\hat{\nabla}\hat{r}|^2 \rangle)_{\hat{r}=1}^2}. \tag{125}$$

Plasmas whose current profiles exhibit strong central peaking tend to have high l_i values, whereas those with broad current profiles tend to have low l_i values.

F. Behavior Close to Magnetic Axis

When $\hat{r} \ll 1$, the well-behaved solution of the axisymmetric ideal-MHD o.d.e.s, (15) and (16), that is dominated by the poloidal harmonic whose poloidal mode number is m is such that

$$y_m(\hat{r}) = \hat{r}^{\,|m|}, \tag{126}$$

$$Z_m(\hat{r}) = |m|\,\hat{r}^{\,|m|}, \tag{127}$$

with $y_{m'}(\hat{r}) = Z_{m'}(\hat{r}) = 0$ for $m' \neq 0$.

VIII. RESULTS

A. Model Equilibria

The model plasma equilibria used in the TJ code are characterized by

$$q_{\mathrm{cly}}(r) = \frac{q(0)\,\nu_q\,\hat{r}^{\,2}}{1 - (1 - \hat{r}^{\,2})^{\nu_q}}, \tag{128}$$

$$p_2(r) = p_2(0)\,(1 - \hat{r}^{\,2})^{\nu_p} \tag{129}$$

for $\hat{r} \leq 1$, and

$$q_{\mathrm{cly}}(r) = q(0)\,\nu_q\,\hat{r}^{\,2} \tag{130}$$

$$p_2(r) = 0 \tag{131}$$

for $\hat{r} > 1$. Here, $q_{\mathrm{cly}}(r)$ is the lowest order (cylindrical) safety-factor profile, whose relation to the actual profile is explained in Ref. 24. The parameter $q(0)$ is the safety-factor on the magnetic axis, whereas the parameter ν_q is automatically adjusted to give a desired value of the safety-factor at the plasma boundary, $q(a)$. Moreover, $p_2(r)$ is the normalized pressure profile [see Eq. (A86)], and $p_2(0)$ controls the central plasma pressure. Note that $q(r)$, $s(r) \equiv d\ln q/d\ln\hat{r}$, and $p_2'(r)$ are all continuous across the plasma-vacuum interface, as is assumed to be the case in our previous analysis, as long as $\nu_q > 1$ and $\nu_p > 1$.
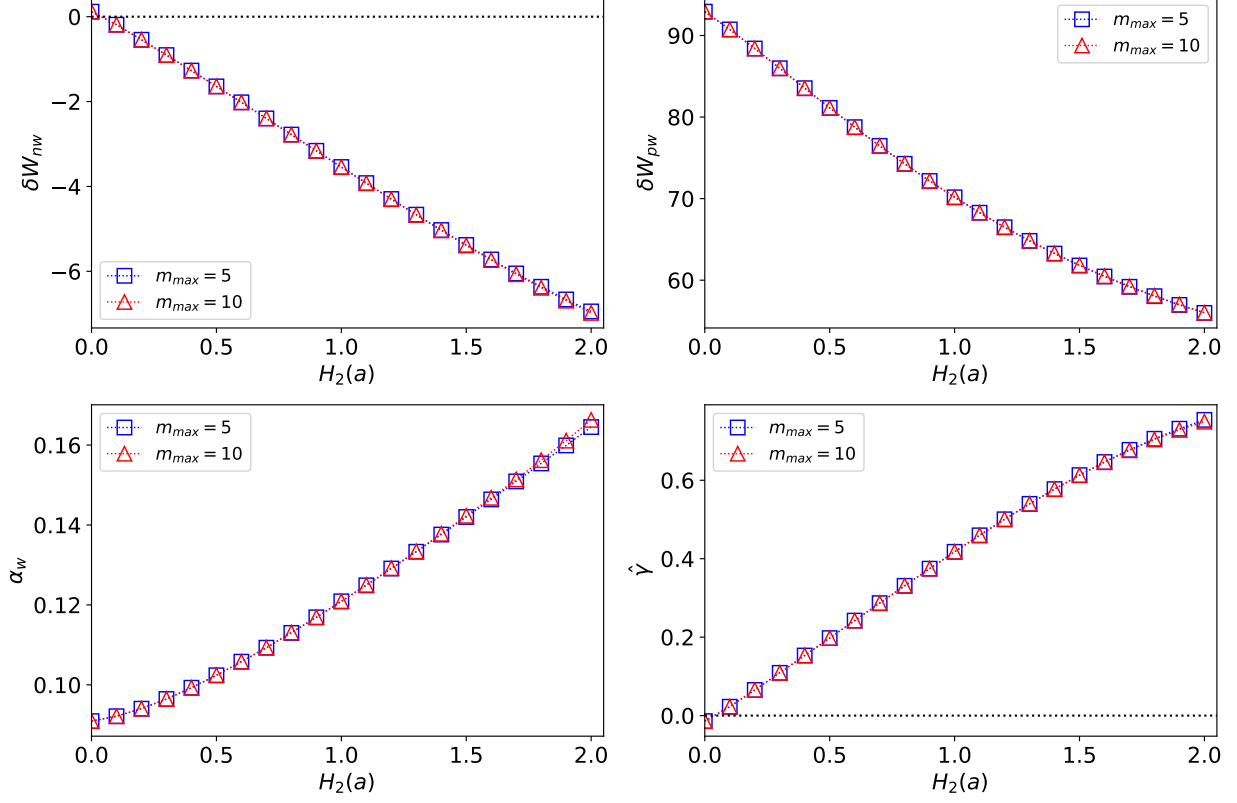
FIG. 1. The no-wall perturbed potential energy, δW_{nw}, the perfect-wall perturbed potential energy, δW_{pw}, the wall parameter, α_w, and the normalized thin-wall growth-rate, $\hat{\gamma}$, of the vertical mode, plotted as functions of the plasma elongation parameter, $H_2(a)$, for plasma equilibria characterized by $\epsilon = 0.1$, $H_3(a) = 0$, $q(0) = 1.01$, $q(a) = 3.6$, $p_2(0) = 0.05$, $\nu_p = 2.5$, and $b_w = 1.1$.

The shaping of the poloidal cross-section of the plasma is determined by two parameters. The first is $H_2(a)$, which controls the plasma elongation. The second is $H_3(a)$, which controls the plasma triangularity. All of the $H_j(a)$ for $j > 3$ are set to zero. Note that, to lowest order, the plasma elongation is $\kappa = 1 + \epsilon H_2(a)$, whereas the plasma triangularity is $\delta = \epsilon H_3(a)$.[24] Moreover, the large aspect-ratio ordering scheme adopted in Sect. VII requires $H_2(a)$ and $H_3(a)$ to be, at most, $\mathcal{O}(1)$ quantities.

In summary, our model equilibria are controlled by eight parameters: $q(0)$, $q(a)$, $p_2(0)$, ν_p, $H_2(a)$, and $H_3(a)$, as well as the inverse aspect-ratio, ϵ, and the relative wall radius, b_w.
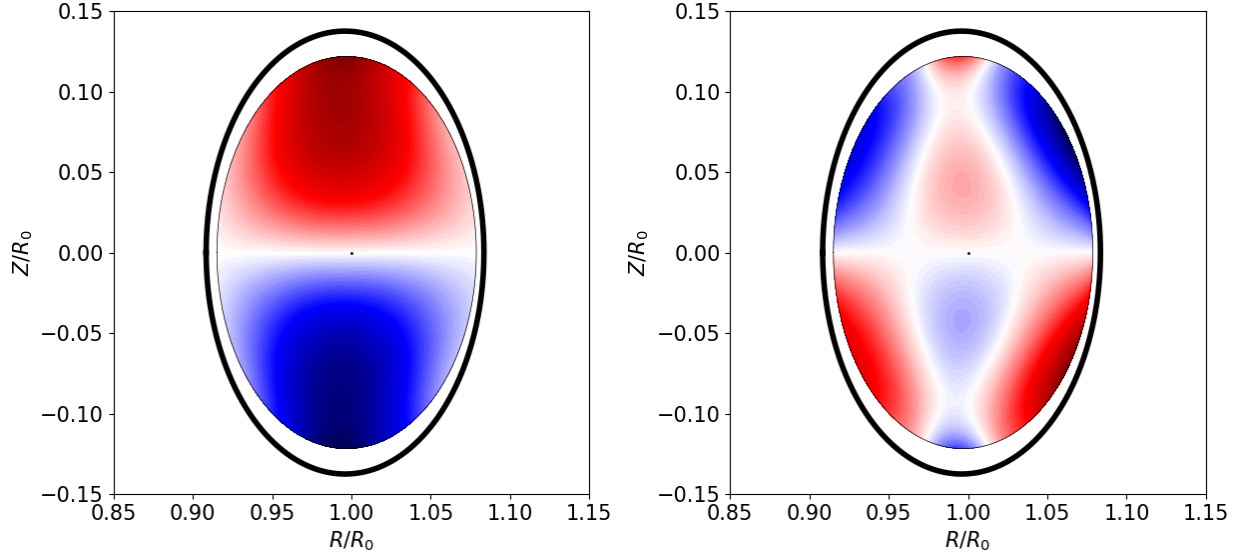
27

FIG. 2. The radial plasma displacement function, $y(r, \theta) = f \, \xi^r$ (left panel), and the perturbed poloidal magnetic field function, $\mathcal{Z}(r, \theta) = -b_\theta$ (right panel), of the vertical mode for the case $H_2(a) = 2$ that features in Fig. 1. Here, red is positive and blue is negative. The thick black line indicates the wall.

B.   Plasma Elongation

Figure 1 shows the variation of the no-wall perturbed potential energy, δW_{nw}, the perfect-wall perturbed plasma energy, δW_{pw}, the wall parameter, α_w [see Eq. (103)], and the normalized growth-rate of the unstable vertical mode, $\hat{\gamma}$, with the elongation parameter, $H_2(a)$, for a series of non-triangular plasmas. Results are shown for $m_{\max} = 5$ (which implies that 11 poloidal harmonics are included in the calculation), and $m_{\max} = 10$ (which implies that 21 poloidal harmonics are included in the calculation). The fact that these results are identical demonstrates that the TJ calculation has achieved convergence with $m_{\max} = 5$. It can be seen that if the plasma cross-section is circular [i.e., if $H_2(a) = 0$] then the vertical mode is stable. However, as soon as the plasma elongation parameter exceeds a very small threshold value the vertical mode becomes unstable.

As is clear from Fig. 2, if the plasma is elongated then the unstable mode causes the plasma to displace vertically. Furthermore, it is apparent from the figure that the unstable
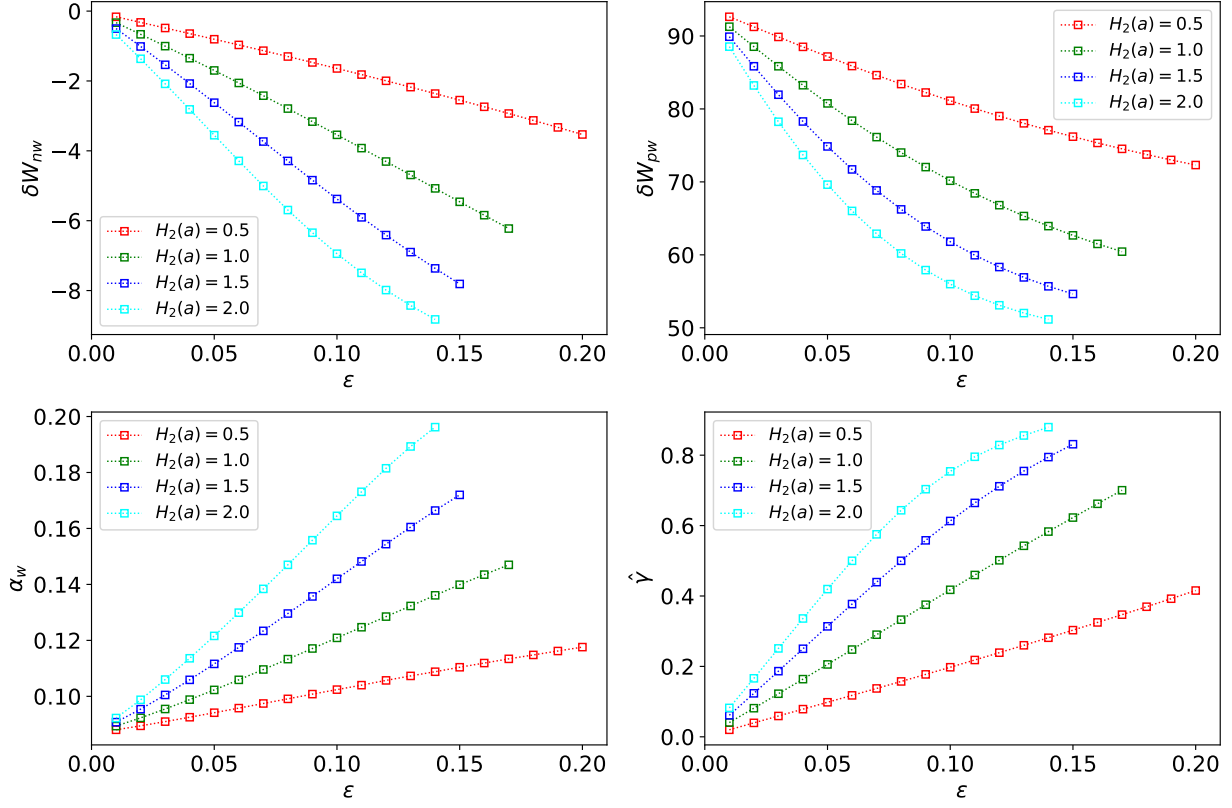
FIG. 3. The no-wall perturbed potential energy, δW_{nw}, the perfect-wall perturbed potential energy, δW_{pw}, the wall parameter, α_w, and the normalized thin-wall growth-rate, $\hat{\gamma}$, of the vertical mode, plotted as functions of the plasma inverse aspect-ratio, ϵ, for plasma equilibria characterized by $H_3(a) = 0$, $q(0) = 1.01$, $q(a) = 3.6$, $p_2(0) = 0.05$, $\nu_p = 2.5$, $b_w = 1.1$, and various different values of $H_2(a)$.

eigenfunction satisfies the constraint (A61). The same can be said for the unstable eigenfunctions shown in Fig. 5.

Of course, the vertical mode needs to be stabilized by means of active feedback. Practical feedback coils must be placed outside the vacuum vessel, which means that the response time of the feedback system is limited by the L/R time of the vessel, τ_w. Realizable feedback systems cannot stabilize the vertical mode if its normalized growth-rate, $\hat{\gamma} = \gamma \tau_w$, exceeds a threshold value that is estimated to be about 1.5.[14] It can be seen that the normalized growth-rates shown in Fig. 1 all lie below this threshold value.

29

C.   Inverse Aspect-Ratio

Figure 3 shows the variation of the no-wall perturbed potential energy, δW_{nw}, the perfect-wall perturbed plasma energy, δW_{pw}, the wall parameter, α_w, and the normalized growth-rate of the unstable vertical mode, $\hat{\gamma}$, with the inverse aspect-ratio, ϵ, for a series of non-triangular plasma equilibria with various different values of the elongation parameter, $H_2(a)$. It can be seen that the growth-rate of the vertical mode initially exhibits a linear increase with increasing inverse aspect-ratio, but that this linear behavior eventually breaks down. Moreover, the breakdown occurs earlier for higher values of $H_2(a)$.

D.   Triangularity

Figure 4 shows the variation of the no-wall perturbed potential energy, δW_{nw}, the perfect-wall perturbed plasma energy, δW_{pw}, the wall parameter, α_w, and the normalized growth-rate of the unstable vertical mode, $\hat{\gamma}$, with the plasma triangularity parameter, $H_3(a)$, for a series of elongated plasma equilibria with various different values of the normalized central pressure, $p_2(0)$. It can be seen that positive triangularity (i.e., a D-shaped plasma cross-section—see Fig. 5) has a stabilizing effect on the vertical mode, whereas negative triangularity has a destabilizing effect. Moreover, whereas positive triangularity plasmas exhibit a mild decrease in the growth-rate of the vertical mode with increasing plasma pressure,[31] negative triangularity plasmas exhibit a strong increase.[32] This finding is significant because, whereas negative triangularity plasma possess many attractive features, such as ELM-free (edge localized mode) operation,[32] their increased susceptibility to the exceptionally dangerous vertical mode is a major drawback. Furthermore, as is clear from right panel of Fig. 5, having a highly conformal wall does not solve the vertical mode problem for negative triangularity plasmas.
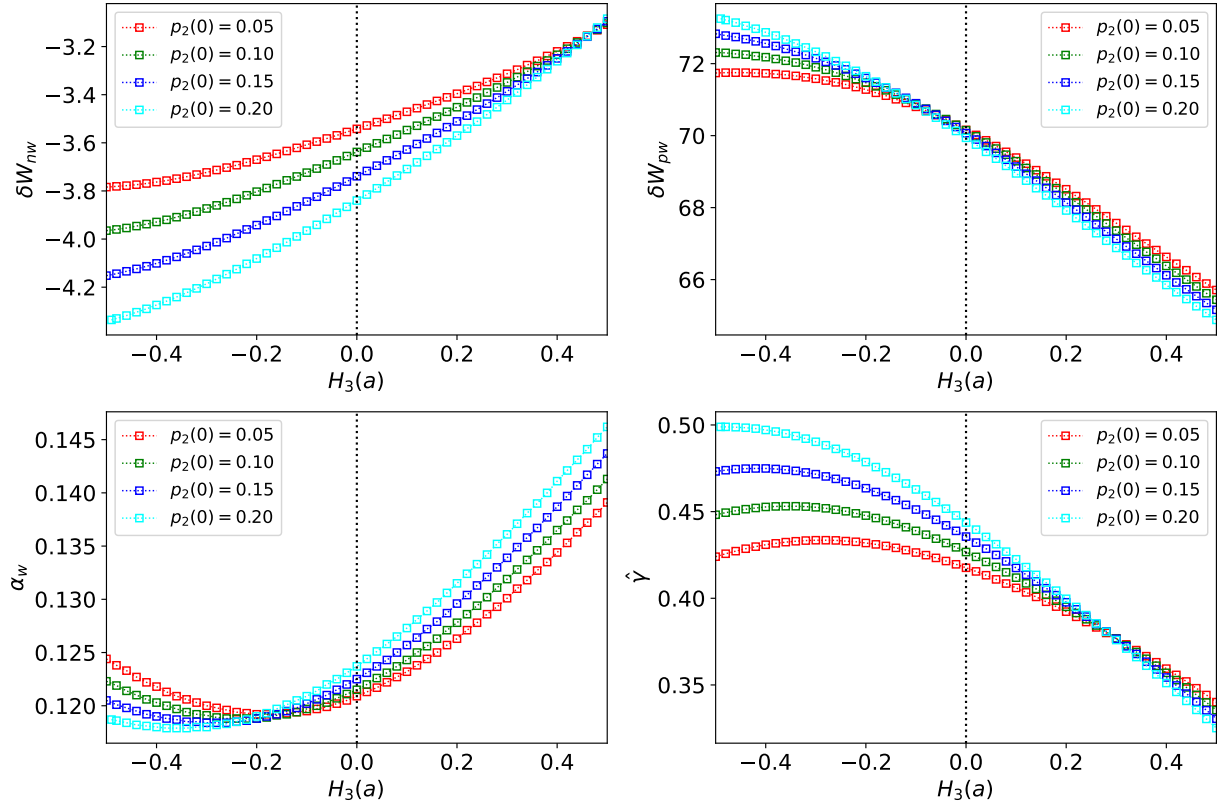
FIG. 4. The no-wall perturbed potential energy, δW_{nw}, the perfect-wall perturbed potential energy, δW_{pw}, the wall parameter, α_w, and the normalized thin-wall growth-rate, $\hat{\gamma}$, of the vertical mode, plotted as functions of the plasma triangularity parameter, $H_3(a)$, for plasma equilibria character-ized by $\epsilon = 0.1$, $H_2(a) = 1$, $q(0) = 1.01$, $q(a) = 3.6$, $\nu_p = 2.5$, $b_w = 1.1$, and various different values of $p_2(0)$.

E. Wall Radius

Figure 6 shows the variation of the no-wall perturbed potential energy, δW_{nw}, the perfect-wall perturbed plasma energy, δW_{pw}, the wall parameter, α_w, and the normalized growth-rate of the unstable vertical mode, $\hat{\gamma}$, with the relative wall radius, b_w, for a series of elongated non-triangular plasma equilibria with various different values of the normalized central pressure, $p_2(0)$. It can be seen that the perfect-wall perturbed plasma energy becomes extremely positive as the wall approaches the plasma boundary (i.e., as $b_w \to 1$). This is indicative
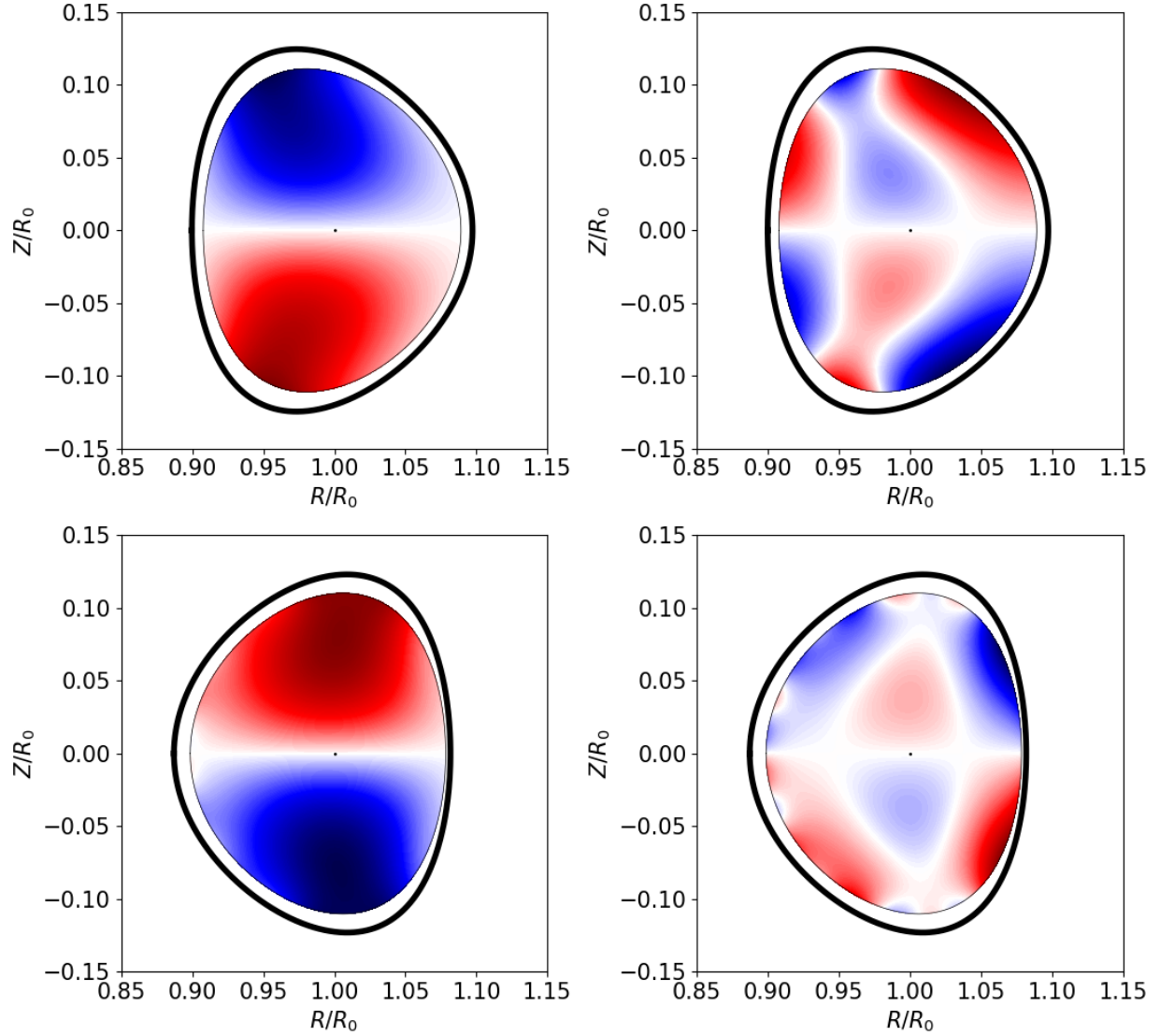
31

FIG. 5. The radial plasma displacement function, $y(r,\theta) = f\,\xi^r$ (left panels), and the perturbed poloidal magnetic field function, $\mathcal{Z}(r,\theta) = -b_\theta$ (right panels), of the vertical mode for the cases $H_3(a) = +0.5$, $p_2(0) = 0.2$ (top panels) and $H_3(a) = -0.5$, $p_2(0) = 0.2$ (bottom panels) that feature in Fig. 4. Here, red is positive and blue is negative. The thick black line indicates the wall.

of the fact that a close-fitting perfectly conducting wall is capable of completely stabilizing any ideal external mode.[20] However, as is clear from the figure, a close-fitting wall does not stabilize the resistive wall mode. In fact, $\hat{\gamma}$ asymptotes to a finite positive value as $b_w \to 1$.
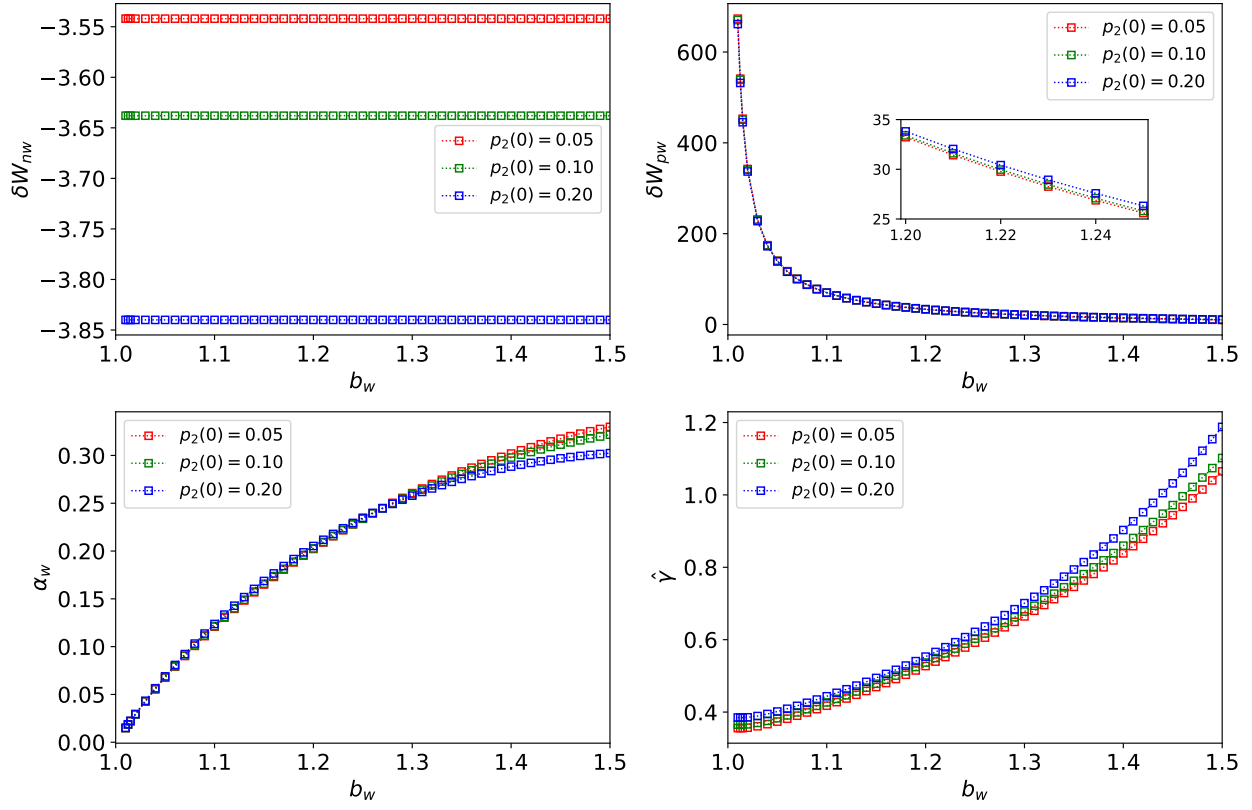
FIG. 6. The no-wall perturbed potential energy, δW_{nw}, the perfect-wall perturbed potential energy, δW_{pw}, the wall parameter, α_w, and the normalized thin-wall growth-rate, $\hat{\gamma}$, of the vertical mode, plotted as functions of the relative wall radius, b_w, for plasma equilibria characterized by $\epsilon = 0.1$, $H_2(a) = 1$, $H_3(a) = 0$, $q(0) = 1.01$, $q(a) = 3.6$, $\nu_p = 2.5$, and various different values of $p_2(0)$.

On the other hand, the growth-rate of the resistive wall mode increases as the wall becomes more distant from the plasma, and quickly attains dangerous levels (i.e., comparable with 1.5). This finding is significant because the vacuum vessel in a tokamak fusion reactor is likely to be quite distant from the plasma because of the presence of shielding material inside the vessel.

F. Internal Inductance

Figure 7 shows the variation of the no-wall perturbed potential energy, δW_{nw}, the perfect-wall perturbed plasma energy, δW_{pw}, the wall parameter, α_w, and the normalized growth-rate of the unstable vertical mode, $\hat{\gamma}$, with the normalized plasma internal inductance, l_i, for a series of elongated plasma equilibria with various different values of triangularity parameter, $H_3(a)$. In practice, the internal inductance is varied by changing $q(0)$ at fixed $q(a)$. It can be seen that non-triangular plasmas exhibit an increase of the growth-rate of the vertical mode with increasing l_i, indicating that the vertical mode is more difficult to stabilize in plasmas with strongly peaked, as opposed to broad, current profiles.[15] Positive triangularity has a marked stabilizing effect on the vertical mode that increases with increasing l_i. Negative triangularity, on the other hand, has a destabilizing effect at low l_i, and a weak stabilizing effect at high l_i.

G. Wall Thickness

All of the results shown up to now in this paper have assumed that the thickness of the wall is much less than its mean minor radius. In fact, as is clear from a comparison of Eqs. (101) and (106), the relationship between the true normalized resistive wall mode growth-rate, $\hat{\gamma}$, and the thin-wall normalized growth-rate, $\hat{\gamma}_{\text{thin}}$, is simply

$$\sqrt{\frac{\hat{\gamma}}{\delta_w}} \tanh\left(\sqrt{\delta_w\,\hat{\gamma}}\right) = \hat{\gamma}_{\text{thin}}, \tag{132}$$

Here, δ_w is the ratio of the wall thickness to the wall mean minor radius. As is clear from Fig. 8, the wall thickness has little influence on the normalized growth-rate of the vertical mode when the growth-rate lies well below the practical threshold value for feedback control, 1.5. On the other hand, finite wall thickness leads to a higher normalized growth-rate when the growth-rate is comparable with the threshold value. This finding suggests that finite wall thickness should be taken into account when calculating the maximum controllable plasma elongation of a tokamak plasma.
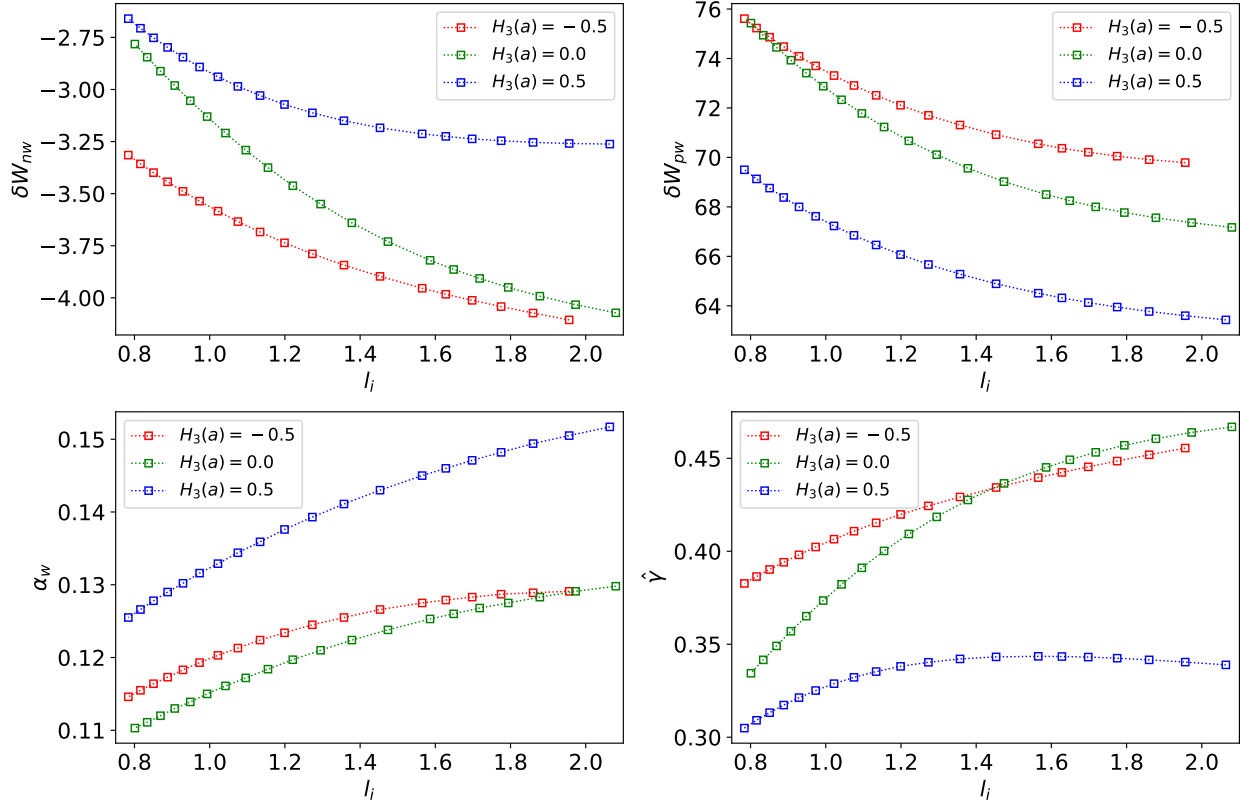
FIG. 7. The no-wall perturbed potential energy, δW_{nw}, the perfect-wall perturbed potential energy, δW_{pw}, the wall parameter, α_w, and the normalized thin-wall growth-rate, $\hat{\gamma}$, of the vertical mode, plotted as functions of the plasma self-inductance, l_i, for plasma equilibria characterized by $\epsilon = 0.1$, $H_2(a) = 1$, $q(a) = 3.6$, $p_2 = 0.05$, $\nu_p = 2.5$, $b_w = 1.1$, and various different values of $H_3(a)$.

IX. SUMMARY

In this paper, we have demonstrated how to calculate the stability of vertical modes in an up-down symmetric, aspect-ratio expanded, tokamak plasma equilibrium surrounded by a conformal resistive wall. The calculation of vertical stability turns out to be significantly different to the calculations of the stability of non-axisymmetric ideal modes in aspect-ratio expanded equilibria described in Refs. 11 and 12. In particular, the role of the toroidal angular momentum flux (which is identically zero for an axisymmetric mode) is instead played by the electromagnetic energy flux. The conservation of electromagnetic energy can be used
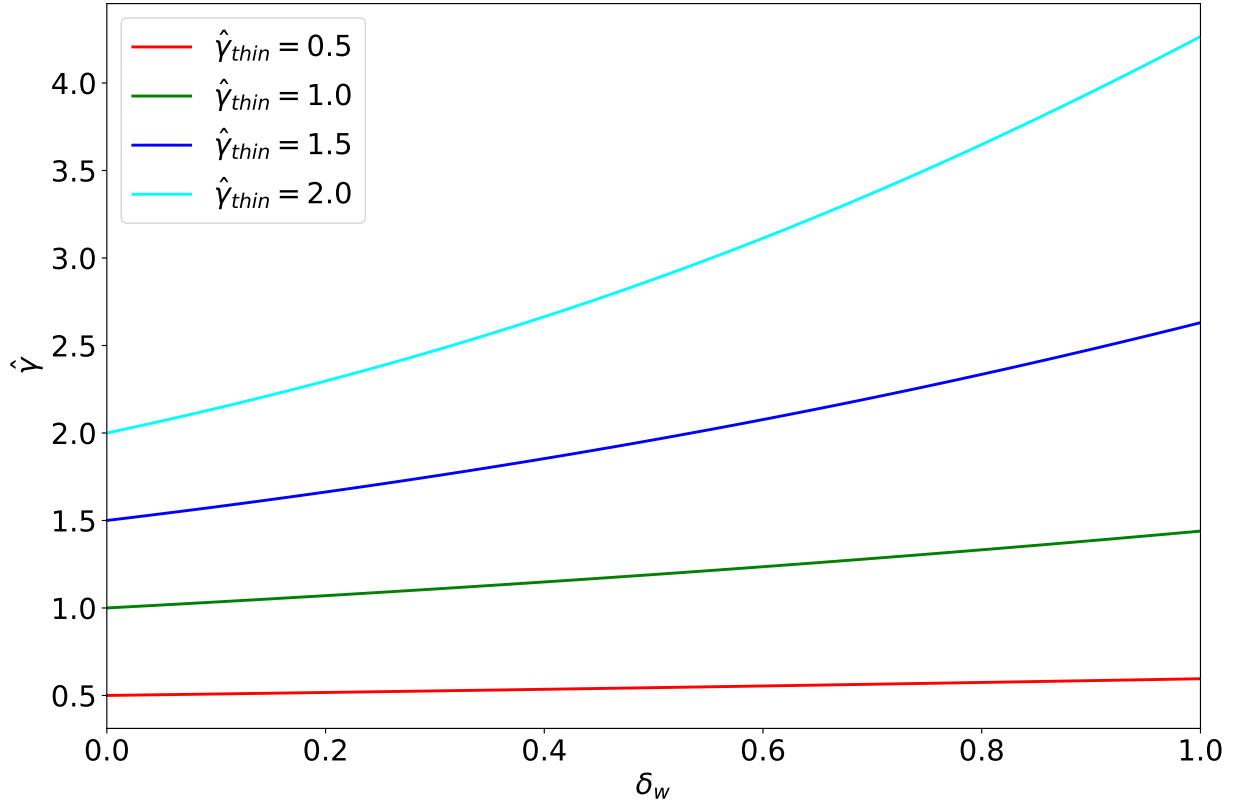
FIG. 8. Variation of the true normalized resistive wall mode growth-rate, $\hat{\gamma}$, with the wall thickness parameter, δ_w, for various values of the thin-wall normalized growth-rate, $\hat{\gamma}_{\mathrm{thin}}$.

to prove that the perturbed plasma potential energy matrix is Hermitian. The calculation described in this paper has been implemented in the TJ toroidal tearing mode code. (This is possible because the basis solutions used to construct tearing eigenfunctions in TJ can be repurposed to construct ideal eigenfunctions.) The results obtained from the enhanced TJ code are broadly similar to those reported previously in the literature.[14,15,21,22,31,32] In particular, positive triangularity is found to have a strong stabilizing effect on the vertical mode, whereas negative triangularity is either destabilizing or weakly stabilizing. Finally, our calculations indicate that finite wall thickness should be taken into account when determining the maximum controllable plasma elongation of a tokamak plasma.

It should be noted that all of the analysis prior to Sect. VII is completely general, and could be used as the basis for the calculation of the stability of a general up-down symmetric

tokamak plasma equilibrium to vertical modes.

ACKNOWLEDGEMENTS

DATA AVAILABILITY STATEMENT

The digital data used in the figures in this paper can be obtained from the author upon reasonable request. The TJ code is freely available at `https://github.com/rfitzp/TJ`.

---

[1] F. Troyon, R. Gruber, H. Saurenmann, S. Semenzato and S. Succi, Plasma Phys. Control. Fusion **26**, 209 (1984).

[2] R. Goldston, Plasma Phys. Control. Fusion **26**, 87 (1984).

[3] M. Huguet, K. Dietz, J.L. Hemmerich and J.R. Last, Fusion Technology **11**, 43 (1987).

[4] M. Okabayashi and G. Sheffield, Nucl. Fusion **14**, 575 (1974).

[5] K. Lackner and A.B. MacMahon, Nucl. Fusion **14**, 575 (1974).

[6] T. Pfirsch and H. Tasso, Nucl. Fusion **11**, 259 (1971).

[7] S.C. Jardin, Phys. Fluids **21**, 1851 (1978).

[8] J.A. Wesson, Nucl. Fusion **18**, 87 (1978).

[9] D. Dobrott and C.S. Chang, Nucl. Fusion **21**, 1573 (1981).

[10] D.J. Ward, S.C. Jardin and C.Z. Cheng, J. Comp. Phys. **104**, 221 (1993).

[11] R. Fitzpatrick, Phys. Plasmas **31**, 102507 (2024).

[12] R. Fitzpatrick, Phys. Plasmas **32**, 062509 (2025).

[13] J.P. Freidberg, A. Cerfon and J.P. Lee, J. Plasma Phys. **81**, 515810608 (2015).

[14] J.P. Lee, A. Cerfon, J.P. Freidberg and M. Greenwald, J. Plasma Phys. **81**, 515810607 (2015).

[15] D.A. Humphreys, N.W. Eidietis, J.R. Ferron, G.L. Jackson, M.J. Lanctot, M.L. Walker, A.S. Welander, G. Raupp, W. Treutterer, P. de Vries, J. Snipes and A. Winter, *Plasma Control Studies Using DIII-D Design Tools in Support of ITER*, 2016 IAEA Fusion Energy Conf. (Kyoto, Japan) [EX/P6-37].

[16] A.H. Boozer, Rev. Mod. Phys. **76**, 1071 (2004).

[17] M.N. Bussac, R. Pellat, D. Edery and J.L. Soule, Phys. Rev. Lett. **35**, 1638 (1975).

[18] J.W. Connor, S.C. Cowley, R.J. Hastie, T.C. Hender, A. Hood and T.J. Martin, Phys. Fluids **31**, 577 (1988).

[19] R. Fitzpatrick, R.J. Hastie, T.J. Martin and C.M. Roach, Nucl. Fusion **33**, 1533 (1993).

[20] J.P. Freidberg, *Ideal Magnetohydrodynamics*, (Plenum, New York NY, 1987).

[21] E. Rebhan and A. Salat, Nucl. Fusion **16**, 805 (1976).

[22] M.D. Rosen, Phys. Fluids **18**, 482 (1975).

[23] R. Fitzpatrick, Phys. Plasmas **31**, 112502 (2024).

[24] R. Fitzpatrick, Phys. Plasmas **31**, 082505 (2024).

[25] S.W. Haney and J.P. Freidberg, Phys. Fluids B **1**, 1637 (1989).

[26] P.M. Morse and H. Feshbach, *Methods of Theoretical Physics*, (McGraw-Hill, New York, NY, 1953), p. 1301.

[27] P.M. Morse and H. Feshbach, *Methods of Theoretical Physics*, (McGraw-Hill, New York, NY, 1953), p. 1302.

[28] M. Abramowitz and I.A. Stegun, *Handbook of Mathematical Functions*, (Dover, New York NY, 1964), sect. 8.11.

[29] M. Abramowitz and I.A. Stegun, *Handbook of Mathematical Functions*, (Dover, New York NY, 1964), chap. 6.

[30] P.M. Morse and H. Feshbach, *Methods of Theoretical Physics*, (McGraw-Hill, New York, NY, 1953), pp. 1302–1309.

[31] D.J. Ward, A. Bondeson and F. Hoffmann, Nucl. Fusion **33**, 821 (1993).

[32] S. Guizzo, A.O. Nelson, C. Hansen, F. Logak and C. Paz-Soldan, Plasma Phys. Control. Fusion **66**, 065018 (2024).

[33] R. Iacono, A. Bondeson, F. Troyon and R. Gruber, Phys. Fluids B **2**, 1794 (1990).

[34] L. Guazzotto, R. Betti, J. Manickam and S. Kaye, Phys. Plasmas **11**, 604 (2004).

Appendix A: Technical Details

1. Wall L/R Time

Let us approximate the wall as a periodic cylinder of length $2\pi\,R_0$, radius b, thickness $d \ll b$, and electrical conductivity σ_w. Let r, θ, z be conventional cylindrical coordinates. In the absence of a plasma, if we imagine that a radially uniform axial current of density $j_0 \sin\theta$ flows in the wall then the wall's self-inductance can easily be shown to take the form $L = \mu_0\,R_0/2$. The electrical resistance of the wall (for an axial current) is $R = R_0/(\sigma_w\,b\,d)$. Hence, the resistive decay time of the current is $L/R = \tau_w/2$, where $\tau_w = \mu_0\,\sigma_w\,b\,d$ is what we shall refer to as the L/R time of the wall.

2. Plasma Equilibrium

It is easily demonstrated from Eq. (4) that [11]

$$B^r = \mathbf{B} \cdot \nabla r = 0, \tag{A1}$$

$$B^\theta = \mathbf{B} \cdot \nabla\theta = \frac{f}{r\,R^2}, \tag{A2}$$

$$B^\phi = \mathbf{B} \cdot \nabla\phi = \frac{g}{R^2} = \frac{q\,f}{r\,R^2}, \tag{A3}$$

$$B_r = \mathcal{J}\,\nabla\theta \times \nabla\phi \cdot \mathbf{B} = -r\,f\,\nabla r \cdot \nabla\theta, \tag{A4}$$

$$B_\theta = \mathcal{J}\,\nabla\phi \times \nabla r \cdot \mathbf{B} = r\,f\,|\nabla r|^2, \tag{A5}$$

$$B_\phi = \mathcal{J}\,\nabla r \times \nabla\theta \cdot \mathbf{B} = g. \tag{A6}$$

The Maxwell equation (neglecting the displacement current, because the plasma velocity perturbations due to axisymmetric modes are far smaller than the velocity of light in vacuum) $\mathbf{J} = \nabla \times \mathbf{B}$ yields

$$\mathcal{J}\,J^r = \frac{\partial B_\phi}{\partial \theta} = 0, \tag{A7}$$

$$\mathcal{J}\,J^\theta = -\frac{\partial B_\phi}{\partial r} = -g', \tag{A8}$$

$$\mathcal{J}\,J^\phi = \frac{\partial B_\theta}{\partial r} - \frac{\partial B_r}{\partial \theta} = \frac{\partial}{\partial r}\left(r\,f\,|\nabla r|^2\right) + \frac{\partial}{\partial \theta}\left(r\,f\,\nabla r \cdot \nabla\theta\right), \tag{A9}$$

where $\mathbf{J}$ is the equilibrium current density, $' \equiv d/dr$, and use has been made of Eqs. (A4)–(A6).

Equilibrium force balance requires that

$$\nabla P = \mathbf{J} \times \mathbf{B}, \tag{A10}$$

where $P(r)$ is the equilibrium scalar plasma pressure. Here, for the sake of simplicity, we have neglected the small centrifugal modifications to force balance due to subsonic plasma rotation.[33,34] It follows that

$$P' = \mathcal{J}(J^\theta\,B^\phi - J^\phi\,B^\theta) = -g'\,\frac{g}{R^2} - \frac{f}{r\,R^2}\left[\frac{\partial}{\partial r}\left(r\,f\,|\nabla r|^2\right) + \frac{\partial}{\partial \theta}\left(r\,f\,\nabla r \cdot \nabla\theta\right)\right], \quad (A11)$$

where use has been made of Eqs. (A1)–(A3), and (A7)–(A9). The other two components of Eq. (A10) are identically zero.

Equation (A11) yields the inverse Grad-Shafranov equation:[18]

$$\frac{f}{r}\frac{\partial}{\partial r}\left(r\,f\,|\nabla r|^2\right) + \frac{f}{r}\frac{\partial}{\partial \theta}\left(r\,f\,\nabla r \cdot \nabla\theta\right) + g\,g' + R^2\,P' = 0. \tag{A12}$$

It follows from Eqs. (5), (A9), and (A12) that

$$\mathcal{J}\,J^\phi = -q\,g' - \frac{r\,R^2\,P'}{f}. \tag{A13}$$

40

It is clear from Eqs. (A8) and (A13) that $g' = P' = 0$ in the current-free "vacuum" region surrounding the plasma, $r \geq a$.

3. Derivation of Axisymmetric Ideal-MHD P.D.E.s

Now,[11]

$$(\boldsymbol{\xi} \times \mathbf{B})_r = \mathcal{J} (\xi^\theta B^\phi - \xi^\phi B^\theta) = f (q\xi^\theta - \xi^\phi), \tag{A14}$$

$$(\boldsymbol{\xi} \times \mathbf{B})_\theta = \mathcal{J} (\xi^\phi B^r - \xi^r B^\phi) = -q f \xi^r, \tag{A15}$$

$$(\boldsymbol{\xi} \times \mathbf{B})_\phi = \mathcal{J} (\xi^r B^\theta - \xi^\theta B^r) = f \xi^r \tag{A16}$$

where use has been made of Eqs. (5) and (A1)–(A3). Combining Eqs. (6) and (A14)–(A16), we obtain [11]

$$\mathcal{J} b^r = \frac{\partial(\boldsymbol{\xi} \times \mathbf{B})_\phi}{\partial \theta} = \frac{\partial(f \xi^r)}{\partial \theta}, \tag{A17}$$

$$\mathcal{J} b^\theta = -\frac{\partial(\boldsymbol{\xi} \times \mathbf{B})_\phi}{\partial r} = -\frac{\partial(f \xi^r)}{\partial r}, \tag{A18}$$

$$\mathcal{J} b^\phi = \frac{\partial(\boldsymbol{\xi} \times \mathbf{B})_\theta}{\partial r} - \frac{\partial(\boldsymbol{\xi} \times \mathbf{B})_r}{\partial \theta} = -\frac{\partial(q f \xi^r)}{\partial r} - \frac{\partial}{\partial \theta}\left[f (q\xi^\theta - \xi^\phi)\right]. \tag{A19}$$

Equations (3), (A17), and (A18) give [11]

$$r R^2 b^r = \frac{\partial y}{\partial \theta}, \tag{A20}$$

$$r R^2 b^\theta = -\frac{\partial y}{\partial r}. \tag{A21}$$

where

$$y(r, \theta) = f \xi^r. \tag{A22}$$

It immediately follows that $\nabla \cdot \mathbf{b} = 0$, in accordance with Eq. (6). Note that Eq. (A21) is radically different from the expression, (54), for b^θ given in Ref. 11. Thus, it is at this stage that our analysis starts to diverge from that of Ref. 11.

According to Eq. (9),

$$p = -P' \nabla r \cdot \boldsymbol{\xi} + \delta p = -P' \xi^r + \delta p. \tag{A23}$$

41

So, the perturbed force balance equation, (7), yields [11]

$$-\frac{\partial\left(P'\,\xi^r\right)}{\partial r} + \frac{\partial\,\delta p}{\partial r} = (\mathbf{j}\times\mathbf{B})_r + (\mathbf{J}\times\mathbf{b})_r, \tag{A24}$$

$$-\frac{\partial\left(P'\,\xi^r\right)}{\partial\theta} + \frac{\partial\,\delta p}{\partial\theta} = (\mathbf{j}\times\mathbf{B})_\theta + (\mathbf{J}\times\mathbf{b})_\theta, \tag{A25}$$

$$0 = (\mathbf{j}\times\mathbf{B})_\phi + (\mathbf{J}\times\mathbf{b})_\phi, \tag{A26}$$

giving [11]

$$-\frac{\partial\left(P'\,\xi^r\right)}{\partial r} + \frac{\partial\,\delta p}{\partial r} = r\,R^2\,(j^\theta\,B^\phi - j^\phi\,B^\theta) + r\,R^2\,(J^\theta\,b^\phi - J^\phi\,b^\theta), \tag{A27}$$

$$-\frac{\partial\left(P'\,\xi^r\right)}{\partial\theta} + \frac{\partial\,\delta p}{\partial\theta} = r\,R^2\,(j^\phi\,B^r - j^r\,B^\phi) + r\,R^2\,(J^\phi\,b^r - J^r\,b^\phi), \tag{A28}$$

$$0 = r\,R^2\,(j^r\,B^\theta - j^\theta\,B^r) + r\,R^2\,(J^r\,b^\theta - J^\theta\,b^r), \tag{A29}$$

where use has been made of Eq. (3). Thus, according to Eqs. (A1)–(A3), (A7), (A8), and (A13),

$$-\frac{\partial\left(P'\,\xi^r\right)}{\partial r} + \frac{\partial\,\delta p}{\partial r} = f\,(q\,j^\theta - j^\phi) - g'\,b^\phi + \left(q\,g' + \frac{r\,R^2\,P'}{f}\right)b^\theta, \tag{A30}$$

$$-\frac{\partial\left(P'\,\xi^r\right)}{\partial\theta} + \frac{\partial\,\delta p}{\partial\theta} = -q\,f\,j^r - \left(q\,g' + \frac{r\,R^2\,P'}{f}\right)b^r, \tag{A31}$$

$$0 = f\,j^r + g'\,b^r. \tag{A32}$$

It follows from Eqs. (A20) and (A32) that

$$r\,R^2\,j^r = -\alpha_g\,\frac{\partial y}{\partial\theta}, \tag{A33}$$

where

$$\alpha_g(r) = \frac{g'}{f}. \tag{A34}$$

Equations (A20), (A22), and (A31) give

$$\delta p = \delta p(r). \tag{A35}$$

Hence, of the three components of the perturbed force balance equation, only Eq. (A30) remains to be solved.

42

Equation (8) yields [11]

$$r\,R^2\,j^r = \frac{\partial b_\phi}{\partial \theta}, \tag{A36}$$

$$r\,R^2\,j^\theta = -\frac{\partial b_\phi}{\partial r}, \tag{A37}$$

$$r\,R^2\,j^\phi = \frac{\partial b_\theta}{\partial r} - \frac{\partial b_r}{\partial \theta}, \tag{A38}$$

where use has been made of Eq. (3). It follows from Eqs. (A33), (A36), and (A37) that

$$b_\phi = -\alpha_g\,y + \delta g(r), \tag{A39}$$

$$r\,R^2\,j^\theta = \frac{\partial(\alpha_g\,y - \delta g)}{\partial r}. \tag{A40}$$

Note that $\nabla \cdot \mathbf{j} = 0$, in accordance with Eq. (8).

Now,

$$\mathbf{b} = b_r\,\nabla r + b_\theta\,\nabla\theta + b_\phi\,\nabla\phi, \tag{A41}$$

so

$$b^r = \mathbf{b} \cdot \nabla r = |\nabla r|^2\,b_r + (\nabla r \cdot \nabla\theta)\,b_\theta, \tag{A42}$$

$$b^\theta = \mathbf{b} \cdot \nabla\theta = (\nabla r \cdot \nabla\theta)\,b_r + |\nabla\theta|^2\,b_\theta, \tag{A43}$$

$$b^\phi = \mathbf{b} \cdot \nabla\phi = \frac{b_\phi}{R^2}. \tag{A44}$$

Equations (3), (A42), and (A43) can be rearranged to give [11]

$$b_r = \left(\frac{1}{|\nabla r|^2}\right) b^r - \left(\frac{\nabla r \cdot \nabla\theta}{|\nabla r|^2}\right) b_\theta, \tag{A45}$$

$$b^\theta = \left(\frac{\nabla r \cdot \nabla\theta}{|\nabla r|^2}\right) b^r + \left(\frac{1}{r^2\,R^2\,|\nabla r|^2}\right) b_\theta. \tag{A46}$$

Let

$$\mathcal{Z}(r,\theta) = |\nabla r|^2\,r\,\frac{\partial y}{\partial r} + r\,\nabla r \cdot \nabla\theta\,\frac{\partial y}{\partial \theta}. \tag{A47}$$

Equations (A20), (A21), (A39), (A45) and (A46) yield

$$b_r = \frac{1}{r\,|\nabla r|^2\,R^2}\frac{\partial y}{\partial \theta} + \frac{\nabla r \cdot \nabla\theta}{|\nabla r|^2}\,\mathcal{Z}, \tag{A48}$$

$$b_\theta = -\mathcal{Z}, \tag{A49}$$

$$b^\phi = -\frac{(\alpha_g\, y - \delta g)}{R^2}. \tag{A50}$$

Equations (A38), (A48), and (A49) give

$$r\, R^2\, j^\phi = -\frac{\partial \mathcal{Z}}{\partial r} - \frac{\partial}{\partial \theta}\left[\frac{1}{r\, |\nabla r|^2\, R^2}\frac{\partial y}{\partial \theta} + \frac{\nabla r \cdot \nabla \theta}{|\nabla r|^2}\,\mathcal{Z}\right]. \tag{A51}$$

It follows from Eqs. (A21), (A22), (A30), (A35), (A40), (A50), and (A51) that

$$-\frac{\partial}{\partial r}\left(\frac{P'}{f}\, y\right) + \delta p' = \frac{f\, q}{r\, R^2}\frac{\partial(\alpha_g\, y - \delta g)}{\partial r} + \frac{f}{r\, R^2}\frac{\partial \mathcal{Z}}{\partial r}$$

$$+\frac{f}{r\, R^2}\frac{\partial}{\partial \theta}\left[\frac{1}{r\, |\nabla r|^2\, R^2}\frac{\partial y}{\partial \theta} + \frac{\nabla r \cdot \nabla \theta}{|\nabla r|^2}\,\mathcal{Z}\right]$$

$$+\frac{g'\,(\alpha_g\, y - \delta g)}{R^2} - \left(q\, g' + \frac{r\, R^2\, P'}{f}\right)\frac{1}{r\, R^2}\frac{\partial y}{\partial r}. \tag{A52}$$

Hence,

$$-\left[(\alpha_f\, \alpha_p + r\, \alpha_p')R^2 + q\, r\, \alpha_g' + r^2\, \alpha_g^2\right] y + \frac{q\, R^2}{g}\, r\, \delta p' + q\, r\, \delta g' + r^2\, \alpha_g\, \delta g$$

$$= r\frac{\partial \mathcal{Z}}{\partial r} + \frac{\partial}{\partial \theta}\left[\frac{1}{|\nabla r|^2\, R^2}\frac{\partial y}{\partial \theta} + \frac{r\, \nabla r \cdot \nabla \theta}{|\nabla r|^2}\,\mathcal{Z}\right], \quad \text{(A53)}$$

and

$$r^2\, R^2\, j^\phi = \left[(\alpha_f\, \alpha_p + r\, \alpha_p')R^2 + q\, r\, \alpha_g' + r^2\, \alpha_g^2\right] y - \frac{q\, R^2}{g}\, r\, \delta p' - q\, r\, \delta g' - r^2\, \alpha_g\, \delta g, \quad \text{(A54)}$$

where

$$\alpha_p(r) = \frac{r\, P'}{f^2}, \tag{A55}$$

$$\alpha_f(r) = \frac{r^2}{f}\frac{d}{dr}\left(\frac{f}{r}\right). \tag{A56}$$

Equations (3), (A19), (A22), and (A50) imply that

$$r\,(\alpha_g\, y - \delta g) = \frac{\partial\,(q\, y)}{\partial r} + \frac{\partial}{\partial \theta}\left[f\,(q\, \xi^\theta - \xi^\phi)\right]. \tag{A57}$$

Hence, we deduce that

$$r\, \delta g = r\, \alpha_g\, \langle y \rangle - \frac{d\,(q\, \langle y \rangle)}{dr}, \tag{A58}$$

44

where $\langle \cdots \rangle = \oint (\cdots) \, d\theta / (2\pi)$. Furthermore, Eqs. (3), (5), (10), and (A22) yield [11]

$$r \, R^2 \, \delta p = -\Gamma \, P \left[\frac{\partial}{\partial r} \left(\frac{q}{g} \, R^2 \, y \right) + \frac{\partial}{\partial \theta} \left(r \, R^2 \, \xi^\theta \right) \right], \tag{A59}$$

which gives

$$r \, \langle R^2 \rangle \, \delta p = -\Gamma \, P \, \frac{d}{dr} \left(\frac{q}{g} \, \langle R^2 \, y \rangle \right). \tag{A60}$$

Let us now assume that

$$\langle y \rangle = \langle R^2 \, y \rangle = 0. \tag{A61}$$

In this case, Eqs. (A58) and (A60) yield

$$\delta g = \delta p = 0, \tag{A62}$$

which, from Eq. (10), implies that $\nabla \cdot \boldsymbol{\xi} = 0$. In other words, the perturbation to the plasma equilibrium does not compress the plasma.

Equations (A47), (A53), and (A62) yield the axisymmetric ideal-MHD partial differential equations (p.d.e.s),

$$r \, \frac{\partial y}{\partial r} = \frac{\mathcal{Z}}{|\nabla r|^2} - \frac{r \, \nabla r \cdot \nabla \theta}{|\nabla r|^2} \, \frac{\partial y}{\partial \theta}, \tag{A63}$$

$$r \, \frac{\partial \mathcal{Z}}{\partial r} = - \left[(\alpha_f \, \alpha_p + r \, \alpha_p') R^2 + q \, r \, \alpha_g' + r^2 \, \alpha_g^2 \right] y - \frac{\partial}{\partial \theta} \left(\frac{1}{|\nabla r|^2 \, R^2} \, \frac{\partial y}{\partial \theta} \right)$$

$$- \frac{\partial}{\partial \theta} \left(\frac{r \, \nabla r \cdot \nabla \theta}{|\nabla r|^2} \, \mathcal{Z} \right), \tag{A64}$$

which govern the perturbed equilibrium.

4. General Coupling Coefficients

The coupling coefficients for the axisymmetric ideal-MHD o.d.e.s are

$$A_m^{m'} = c_m^{m'}, \tag{A65}$$

$$B_m^{m'} = -m' \, f_m^{m'}, \tag{A66}$$

$$C_m^{m'} = -m \, f_m^{m'}, \tag{A67}$$

$$D_m^{m'} = -(\alpha_f \, \alpha_p + r \, \alpha_p') \, a_m^{m'} - (q \, r \, \alpha_g' + r^2 \, \alpha_g^2) \, \delta_m^{m'} + m \, m' \, b_m^{m'}, \tag{A68}$$

where

$$a_m^{m'}(r) = \oint R^2 \exp[-\mathrm{i}\,(m - m')\,\theta]\,\frac{d\theta}{2\pi}, \tag{A69}$$

$$b_m^{m'}(r) = \oint |\nabla r|^{-2}\,R^{-2}\,\exp[-\mathrm{i}\,(m - m')\,\theta]\,\frac{d\theta}{2\pi}, \tag{A70}$$

$$c_m^{m'}(r) = \oint |\nabla r|^{-2}\,\exp[-\mathrm{i}\,(m - m')\,\theta]\,\frac{d\theta}{2\pi}, \tag{A71}$$

$$f_m^{m'}(r) = \oint \frac{\mathrm{i}\,r\,\nabla r \cdot \nabla\theta}{|\nabla r|^2}\,\exp[-\mathrm{i}\,(m - m')\,\theta]\,\frac{d\theta}{2\pi}. \tag{A72}$$

Here, $\delta_m^{m'}$ is a Kronecker delta symbol.

Note that $a_{m'}^m = a_m^{m'*}$, $b_{m'}^m = b_m^{m'*}$, $c_{m'}^m = c_m^{m'*}$, and $f_{m'}^m = -f_m^{m'*}$, which implies that $A_{m'}^m = A_{m'}^{m*}$, $B_{m'}^m = -C_{m'}^{m*}$, $C_{m'}^m = -B_{m'}^{m*}$, and $D_{m'}^m = D_{m'}^{m*}$.

5.   Derivation of Large Aspect-Ratio Coupling Coefficients

a.   Coordinate Transformation

Let

$$J(\hat{r}, \omega) = \frac{1}{\epsilon^2}\left(\frac{\partial R}{\partial \omega}\frac{\partial Z}{\partial \hat{r}} - \frac{\partial R}{\partial \hat{r}}\frac{\partial Z}{\partial \omega}\right) \tag{A73}$$

be the Jacobian of the $\hat{r}$, ω coordinate system. We can transform to the $\hat{r}$, θ coordinate system by writing

$$\theta(\hat{r}, \omega) = 2\pi \int_0^\omega \frac{J(\hat{r}, \tilde{\omega})}{R(\hat{r}, \tilde{\omega})}\,d\tilde{\omega} \bigg/ \oint \frac{J(\hat{r}, \omega)}{R(\hat{r}, \omega)}\,d\omega, \tag{A74}$$

$$\hat{r} = \frac{1}{2\pi}\oint \frac{J(\hat{r}, \omega)}{R(\hat{r}, \omega)}\,d\omega. \tag{A75}$$

This transformation ensures that

$$\frac{\partial \theta}{\partial \omega} = \frac{J}{\hat{r}\,R}, \tag{A76}$$

and, hence, that

$$\mathcal{J} \equiv \frac{R}{\epsilon}\left(\frac{\partial R}{\partial \theta}\frac{\partial Z}{\partial \hat{r}} - \frac{\partial R}{\partial \hat{r}}\frac{\partial Z}{\partial \hat{r}}\right) = \epsilon\,R\,J\,\frac{\partial \omega}{\partial \theta} = r\,R^2, \tag{A77}$$

in accordance with Eq. (3). Note, from Eqs. (A75) and (A76) that

$$\hat{r} = \frac{1}{2\pi}\oint \hat{r}\,\frac{\partial \theta}{\partial \omega}\,d\omega = \hat{r}. \tag{A78}$$

Thus, the transformation (A74) and (A75) really does transform between the $\hat{r}$, ω and the $\hat{r}$, θ coordinate systems.

b.   Metric Elements

We can determine the metric elements of the flux-coordinate system by combining Eqs. (107), (108), and (A73)–(A75). Evaluating the elements up to $\mathcal{O}(\epsilon)$, but retaining $\mathcal{O}(\epsilon^2)$ contributions to terms that are independent of ω, we obtain,[11,12]

$$L(\hat{r}) = \frac{\hat{r}^3}{8} - \frac{\hat{r}\,H_1}{2} - \frac{1}{2}\sum_{j>1}(j-1)\,\frac{H_j^2}{\hat{r}}, \tag{A79}$$

$$\theta = \omega + \epsilon\,\hat{r}\,\sin\omega - \epsilon\sum_{j>0}\frac{1}{j}\left[H_j' - (j-1)\,\frac{H_j}{\hat{r}}\right]\sin(j\,\omega), \tag{A80}$$

$$|\hat{\nabla}\hat{r}|^2 = 1 + 2\,\epsilon\sum_{j>0}H_j'\,\cos(j\,\theta)$$
$$+ \epsilon^2\left(\frac{3\,\hat{r}'^2}{4} - H_1 + \frac{1}{2}\sum_{j>0}\left[H_j'^2 + (j^2-1)\,\frac{H_j^2}{\hat{r}^2}\right]\right), \tag{A81}$$

$$\hat{\nabla}\hat{r}\cdot\hat{\nabla}\theta = \epsilon\,\sin\theta - \epsilon\sum_{j>0}\frac{1}{j}\left[H_j'' + \frac{H_j'}{\hat{r}} + (j^2-1)\,\frac{H_j}{\hat{r}^2}\right]\sin(j\,\theta), \tag{A82}$$

$$R^2 = 1 - 2\,\epsilon\,\hat{r}\,\cos\theta - \epsilon^2\left(\frac{\hat{r}^2}{2} - \hat{r}\,H_1' - 2\,H_1\right). \tag{A83}$$

Here, $' \equiv d/d\hat{r}$.

c.   Expansion of Inverse Grad-Shafranov Equation

Let us write [11,12]

$$f(\hat{r}) = \epsilon\,\frac{\hat{r}\,g}{q}, \tag{A84}$$

$$g(\hat{r}) = 1 + \epsilon^2\,g_2(\hat{r}) + \epsilon^4\,g_4(\hat{r}), \tag{A85}$$

$$P'(\hat{r}) = \epsilon^2\,p_2'(\hat{r}), \tag{A86}$$

where q, g_2, g_4, and p_2 are all $\mathcal{O}(1)$. Here, the safety-factor, $q(\hat{r})$, and the second-order plasma pressure gradient, $p_2'(\hat{r})$, are the two free flux-surface functions that characterize the plasma equilibrium.

Expanding the inverse Grad-Shafranov equation, (A12), order by order in the small parameter ϵ, making use of Eqs. (A81)–(A86), we obtain [11,12,19]

$$g_2' = -p_2' - \frac{\hat{r}}{q^2}\,(2 - s), \tag{A87}$$

$$H_1'' = -(3 - 2\,s)\,\frac{H_1'}{\hat{r}} - 1 + \frac{2\,p_2'\,q^2}{\hat{r}}, \tag{A88}$$

$$H_j'' = -(3 - 2\,s)\,\frac{H_j'}{\hat{r}} + (j^2 - 1)\,\frac{H_j}{\hat{r}^2} \qquad \text{for } j > 1, \tag{A89}$$

$$g_4' = g_2\left[p_2' - \frac{\hat{r}}{q^2}\,(2 - s)\right] - \frac{\hat{r}}{q}\,\Sigma + p_2'\left(\frac{\hat{r}^2}{2} + \frac{\hat{r}^2}{q^2} - 2\,H_1 - 3\,\hat{r}\,H_1'\right), \tag{A90}$$

where $s = \hat{r}\,q'/q$ is the magnetic shear, and

$$\Sigma = \frac{S_2}{q} - \frac{2 - s}{q}\,S_3, \tag{A91}$$

$$S_1(\hat{r}) = \frac{1}{2}\sum_{j>0}\left[3\,H_j'^{\,2} - (j^2 - 1)\,\frac{H_j^{\,2}}{\hat{r}^2}\right], \tag{A92}$$

$$S_2(\hat{r}) = \frac{3\,\hat{r}^{\,2}}{2} - 2\,\hat{r}\,H_1' + \sum_{j>0}\left[H_j'^{\,2} + 2\,(j^2 - 1)\,\frac{H_j'\,H_j}{\hat{r}} - (j^2 - 1)\,\frac{H_j^{\,2}}{\hat{r}^{\,2}}\right], \tag{A93}$$

$$S_3(\hat{r}) = -\frac{3\,\hat{r}^{\,2}}{4} + \frac{\hat{r}^{\,2}}{q^2} + H_1 + S_1, \tag{A94}$$

$$S_4(\hat{r}) = \frac{7\,\hat{r}^{\,2}}{4} - H_1 - 3\,\hat{r}\,H_1' + S_1. \tag{A95}$$

The horizontal *Shafranov shift* of equilibrium magnetic flux-surfaces is parameterized by $-H_1$. Note that H_1 is driven by toroidicity [the second term on the right-hand side of Eq. (A88)], and plasma pressure gradients (the third term). All of the other shaping terms (i.e., the H_j for $j > 1$) are driven by axisymmetric currents flowing in external magnetic field-coils.

Equations (A34), (A55), (A56), and (A84)–(A86) yield [11]

$$\alpha_p(\hat{r}) = \frac{p_2'\,q^2}{\hat{r}}\left(1 - 2\,\epsilon^2\,g_2\right), \tag{A96}$$

$$\alpha_g(\hat{r}) = \frac{q}{\hat{r}} \left(g_2' - \epsilon^2 \, g_2 \, g_2' + \epsilon^2 \, g_4' \right), \tag{A97}$$

$$\alpha_f(\hat{r}) = -s + \epsilon^2 \, \hat{r} \, g_2'. \tag{A98}$$

Finally, it follows from Eqs. (A82) and (A88)–(A89) that

$$\hat{\nabla}\hat{r} \cdot \hat{\nabla}\theta = 2\,\epsilon \left[1 - \frac{p_2' \, q^2}{\hat{r}} + (1 - s) \, \frac{H_1'}{\hat{r}} \right] \sin\theta$$
$$- 2\,\epsilon \sum_{j>1} \frac{1}{j} \left[-(1 - s) \, \frac{H_j'}{\hat{r}} + (j^2 - 1) \, \frac{H_j}{\hat{r}^2} \right] \sin(j\,\theta). \tag{A99}$$

<div align="center">

d.   Calculation of Coupling Coefficients

</div>

Equations (A81) and (A92) yield

$$|\hat{\nabla}\hat{r}|^{-2} = 1 - 2\,\epsilon \sum_{j>0} H_j' \, \cos(j\,\theta) + \epsilon^2 \left(-\frac{3\,\hat{r}^2}{4} + H_1 + S_1 \right), \tag{A100}$$

Equation (A83) gives

$$R^{-2} = 1 + 2\,\epsilon\,\hat{r}\,\cos\theta + \epsilon^2 \left(\frac{5\,\hat{r}^2}{2} - \hat{r}\,H_1' - 2\,H_1 \right). \tag{A101}$$

The previous two equations imply that

$$|\hat{\nabla}\hat{r}|^{-2} R^{-2} = 1 + 2\,\epsilon\,\hat{r}\,\cos\theta - 2\,\epsilon \sum_{j>0} H_j' \, \cos(j\,\theta) + \epsilon^2 \left(\frac{7\,\hat{r}^2}{4} - H_1 - 3\,\hat{r}\,H_1' + S_1 \right). \tag{A102}$$

Finally, Eqs. (A99) and (A100) yield

$$\hat{\nabla}\hat{r} \cdot \hat{\nabla}\theta \, |\hat{\nabla}\hat{r}|^{-2} = 2\,\epsilon \left[1 - \frac{p_2' \, q^2}{\hat{r}} + (1 - s) \, \frac{H_1'}{\hat{r}} \right] \sin\theta$$
$$- 2\,\epsilon \sum_{j>1} \frac{1}{j} \left[-(1 - s) \, \frac{H_j'}{\hat{r}} + (j^2 - 1) \, \frac{H_j}{\hat{r}^2} \right] \sin(j\,\theta). \tag{A103}$$

Equations (A69)–(A72), (A83), (A100), (A102), and (A103) imply that

$$a_m^{m'} = \delta_m^{m'} - \epsilon\,\hat{r} \left(\delta_{m'-m-1} + \delta_{m'-m+1} \right) - \epsilon^2 \left(\frac{\hat{r}^2}{2} - \hat{r}\,H_1' - 2\,H_1 \right) \delta_m^{m'}, \tag{A104}$$

$$b_m^{m'} = \delta_m^{m'} + \epsilon\,\hat{r} \left(\delta_{m'-m-1} + \delta_{m'-m+1} \right) - \epsilon \sum_{j>0} H_j' \left(\delta_{m'-m-j} + \delta_{m'-m+j} \right)$$

$$+ \epsilon^2 \left(\frac{7 \hat{r}^2}{4} - H_1 - 3 \hat{r} H_1' + S_1 \right) \delta_m^{m'}, \tag{A105}$$

$$c_m^{m'} = \delta_m^{m'} - \epsilon \sum_{j>0} H_j' \left(\delta_{m'-m-j} + \delta_{m'-m+j} \right) + \epsilon^2 \left(-\frac{3 \hat{r}^2}{4} + H_1 + S_1 \right) \delta_m^{m'}, \tag{A106}$$

$$f_m^{m'} = -\epsilon \left[\hat{r} - p_2' q^2 + (1-s) H_1' \right] \left(\delta_{m'-m-1} - \delta_{m'-m+1} \right)$$

$$+ \epsilon \sum_{j>1} \frac{1}{j} \left[-(1-s) H_j' + (j^2 - 1) \frac{H_j}{\hat{r}} \right] \left(\delta_{m'-m-j} - \delta_{m'-m+j} \right). \tag{A107}$$

If we write

$$\alpha_g = \alpha_g^{(0)} + \epsilon^2 \alpha_g^{(2)}, \tag{A108}$$

$$\alpha_p = \alpha_p^{(0)} + \epsilon^2 \alpha_p^{(2)}, \tag{A109}$$

$$\alpha_f = \alpha_f^{(0)} + \epsilon^2 \alpha_f^{(2)}, \tag{A110}$$

$$a_m^{m'} = 1 + \epsilon \, a_m^{m' \, (1)} + \epsilon^2 \, a_m^{m' \, (2)}, \tag{A111}$$

$$b_m^{m'} = 1 + \epsilon \, b_m^{m' \, (1)} + \epsilon^2 \, b_m^{m' \, (2)}, \tag{A112}$$

$$D_m^{m'} = D_m^{m' \, (0)} + \epsilon \, D_m^{m' \, (1)} + \epsilon^2 \, D_m^{m' \, (2)}, \tag{A113}$$

where $\alpha_g^{(0)}$, $\alpha_g^{(2)}$, et cetera, are $\mathcal{O}(1)$, then it follows from Eq. (A68) that

$$D_m^{m \, (0)} = -\alpha_f^{(0)} \alpha_p^{(0)} - \hat{r} \alpha_p'^{(0)} - q \hat{r} \alpha_g'^{(0)} + m^2, \tag{A114}$$

$$D_m^{m' \, (1)} = - \left[\alpha_f^{(0)} \alpha_p^{(0)} + \hat{r} \alpha_p'^{(0)} \right] a_m^{m' \, (1)} + m \, m' \, b_m^{m' \, (1)}, \tag{A115}$$

$$D_m^{m \, (2)} = - \left[\alpha_f^{(0)} \alpha_p^{(0)} + \hat{r} \alpha_p'^{(0)} \right] a_m^{m' \, (2)} - \alpha_f^{(0)} \alpha_p^{(2)} - \alpha_f^{(2)} \alpha_p^{(0)} - \hat{r} \alpha_p'^{(2)} - q \hat{r} \alpha_g'^{(2)}$$

$$- \hat{r}^2 \left[\alpha_g^{(0)} \right]^2 + m^2 \, b_m^{m \, (2)}. \tag{A116}$$

Finally, Eqs. (A69)–(A72), (A104)–(A107), and (A114)–(A116) give the following expressions for the coupling coefficients appearing in the axisymmetric ideal-MHD o.d.e.s, (15) and (16):

$$A_m^m(\hat{r}) = 1 + \epsilon^2 \left(-\frac{3 \hat{r}^2}{4} + H_1 + S_1 \right), \tag{A117}$$

$$A_m^{m \pm 1}(\hat{r}) = -\epsilon H_1', \tag{A118}$$

$$A_m^{m\pm j}(\hat{r}) = -\epsilon\, H_j' \qquad \text{for } j > 1, \tag{A119}$$

$$B_m^m(\hat{r}) = 0, \tag{A120}$$

$$B_m^{m\pm 1}(\hat{r}) = \pm\epsilon\,(m\pm 1)\left[\hat{r} - p_2'\,q^2 + (1-s)\,H_1'\right], \tag{A121}$$

$$B_m^{m\pm j}(\hat{r}) = \pm\epsilon\,\frac{m\pm j}{j}\left[(1-s)\,H_j' - (j^2-1)\,\frac{H_j}{\hat{r}}\right] \qquad \text{for } j > 1, \tag{A122}$$

$$C_m^m(\hat{r}) = 0, \tag{A123}$$

$$C_m^{m\pm 1}(\hat{r}) = \pm\epsilon\, m\left[\hat{r} - p_2'\,q^2 + (1-s)\,H_1'\right], \tag{A124}$$

$$C_m^{m\pm j}(\hat{r}) = \pm\epsilon\,\frac{m}{j}\left[(1-s)\,H_j' - (j^2-1)\,\frac{H_j}{\hat{r}}\right] \qquad \text{for } j > 1, \tag{A125}$$

$$D_m^m(\hat{r}) = m^2 + q\,\hat{r}\,\frac{d}{d\hat{r}}\left(\frac{2-s}{q}\right) + \epsilon^2\, m^2\, S_4$$

$$+ \epsilon^2\left\{-\hat{r}^2\left(\frac{2-s}{q}\right)^2 + q\,\hat{r}\,\frac{d\Sigma}{d\hat{r}} - \hat{r}\,\frac{d}{d\hat{r}}(\hat{r}\,p_2') - 2\,(1-s)\,\hat{r}\,p_2'\right.$$

$$\left. +2\,\hat{r}\,p_2'\,q^2\left(-2 + \frac{3\,p_2'\,q^2}{\hat{r}}\right) + 2\,H_1'\,q^2\left[\frac{d}{d\hat{r}}(\hat{r}\,p_2') - 4\,(1-s)\,p_2'\right]\right\}, \tag{A126}$$

$$D_m^{m\pm 1}(\hat{r}) = \epsilon\,q^2\left[\frac{d}{d\hat{r}}(\hat{r}\,p_2') - (2-s)\,p_2'\right] + \epsilon\, m\,(m\pm 1)\,(\hat{r} - H_1'), \tag{A127}$$

$$D_m^{m\pm j}(\hat{r}) = -\epsilon\, m\,(m\pm j)\,H_j' \qquad \text{for } j > 1. \tag{A128}$$